Modeling of Thermoplastic Composite Filament Winding

Xiaolan Song

Thesis submitted to the Faculty of the
Virginia Polytechnic Institute and State University
in partial fulfillment of the requirements for the degree of

Master of Science
in
Engineering Science and Mechanics

Dr. Alfred C. Loos, Chair
Dr. Romesh C. Batra
Dr. Zafer Gurdal

September 29, 2000
Blacksburg, Virginia

Key words: Thermoplastic composite filament winding, on-line connsolidation, modeling

Modeling of Thermoplastic Composite Filament Winding

Xiaolan Song

(Abstract)

Thermoplastic composite filament winding is an on-line consolidation process, where the composite experiences a complex temperature history and undergoes a number of temperature history affected microstructural changes that influence the structure's subsequent properties. These changes include melting, crystallization, void formation, degradation and consolidation. In the present study, models of the thermoplastic filament winding process were developed to identify and understand the relationships between process variables and the structure quality. These include models that describe the heat transfer, consolidation and crystallization processes that occur during fabrication of a filament wound composites structure.

A comprehensive thermal model of the thermoplastic filament winding process was developed to calculate the temperature profiles in the composite substrate and the towpreg temperature before entering the nippoint. A two-dimensional finite element heat transfer analysis for the composite-mandrel assembly was formulated in the polar coordinate system, which facilitates the description of the geometry and the boundary conditions. A four-node 'sector element' was used to describe the domain of interest. Sector elements were selected to give a better representation of the curved boundary shape which should improve accuracy with fewer elements compared to a finite element solution in the Cartesian-coordinate system. Hence the computational cost will be reduced. The second thermal analysis was a two-dimensional, Cartesian coordinate, finite element model of the towpreg as it enters the nippoint. The results show that the calculated temperature distribution in the composite substrate compared well with temperature data measured during winding and consolidation. The analysis also agrees with the experimental observation that the melt region is formed on the surface of the incoming towpreg in the nippoint and not on the substrate.

Incorporated with the heat transfer analysis were the consolidation and crystallization models. These models were used to calculate the degree of interply bonding and the crystallinity achieved during composite manufacture. Bonding and crystallinity developments during the winding process were investigated using the model. It is concluded that lower winding speed, higher hot-air heater nozzle temperature, and higher substrate preheating temperature yield higher nippoint temperature, better consolidation and a higher degree of crystallization. Complete consolidation and higher matrix crystallization will result in higher interlaminar strength of the wound composite structure.

Acknowledgements

First, I would like to thank the members of my Advisory Committee: Dr. Alfred C. Loos, Dr. Romesh C. Batra, and Dr. Zafer Gurdal, for their time and expertise. I would also like to thank Dr. Po-Jen Shih, who provided all the experimental data and gave me much help in the work. Lastly, I would like to thank Luna Innovations for their generous funding and support.

Table of Contents

List of Figures

List of Tables

Chapter 1 Introduction

The filament winding process is a low-cost, automated composite manufacturing technique. A continuous reinforcement is impregnated with resin and laid down on the surface of a rotating mandrel along a predetermined path. The matrix materials can be either thermoset or thermoplastic resins. Thermoplastic filament winding offers the additional advantage of on-line consolidation, where the resin impregnated fiber bundles are continuously oriented, laid down, and, consolidated onto the tool surface in a single step. When integrated with a computer-controlled system, the process can be fully automated resulting in additional cost savings by increasing productivity and reducing labor cost.

The use of thermoplastic resin eliminates the need for high temperature cure of the entire structure in an autoclave or convection oven which minimizes the build-up of residual stress in thick-section parts caused by large volumetric changes during the post-processing [1]. High-levels of residual stresses may lead to dimensional instability and premature failure [2-4]. Hence, the on-line consolidation process has the potential to produce better quality composite structures.

In addition to the above-mentioned advantages, thermoplastic filament winding offers benefits for design flexibility and performance. With localized heating, this process is suitable for manufacturing parts with large surfaces and moderate curvatures, such as fuselage structures and deep submersibles [5]. Because the towpreg is fully consolidated and locked in the vicinity of the melting point as it is placed onto the structure, conceptually there is no limitation on producing parts with thick cross-sections and large surface areas [6]. Furthermore, complex, non-geodesic, and even concave winding paths are achievable, thus allowing design flexibility [7].

The basic components of on-line consolidation process are illustrated in Figure 1.1. A focused heat source is aimed at the interface between the incoming towpreg and substrate and creates a molten zone. Once the proper molten zone has been created, pressure is applied via the compaction roller which results in flow and deformation of the resin impregnated fiber tow. Once intimate contact between the mating surfaces is

achieved, bonding of the towpreg/substrate interface occurs by autohesion. The roller pressure should be applied until the temperature of the bonded interface drops below the melting/softening point of the resin in order to prevent void formation by either volumetric shrinkage or the release of spring energy from the fiber network.

Thermoplastic filament winding is a nonisothermal manufacturing process where the composite experiences a complex temperature history. The composite substrate is repeatedly heated and cooled as additional layers are wound onto the structure. This thermal cycling can cause microstructural changes that influence the structure's properties. These changes include melting, crystallization, void formation, degradation and consolidation. Therefore, a comprehensive heat transfer analysis must be developed to predict and understand the rapid temperature changes associated with the manufacturing process.

In the thermoplastic filament winding process, the rate of consolidation depends on the time required to achieve intimate contact and complete autohesive bonding strength at the interface between the towpreg and the composite substrate. In general, the winding speed,

heat source intensity, and roller pressure are the key variables that determine the processing window.

It is well recognized that the surfaces of towpregs are uneven. Under the proper pressure and heat, the viscous matrix is compressed, the gaps at the interface are filled and perfect contact is formed. This mechanism is identified as intimate contact formation. Once two adjacent interfaces come into contact, the mechanism of autohesion controls the interply bond formation. Polymer chains of amorphous thermoplastics above the glass transition temperature or semicrystalline thermoplastics above the melt temperature diffuse across the interface and entangles with molecular chains on the other side of the interface, so that the interface is no longer distinguishable from the bulk polymer. The resulting bond strength is a function of the processing parameters (temperature, pressure and time) to which the interface is subjected. Individual plies consolidate into a laminate by bonding at the interfaces. The two major mechanisms governing the development of

interply bonding, intimate contact and autohesion, are believed to occur sequentially or simultaneously.

The final step of thermoplastic composite consolidation is to cool and solidify the consolidated parts. For semicrystalline thermoplastics, crystallization occurs during cooling. The cooling rate has been identified as the most important influence on the morphology of the matrix and the degree of crystallinity. In general, slower cooling rates yield higher degrees of crystallinity which correspond to an increase in tensile strength, compressive strength, and solvent resistance of the matrix. As the temperature history that the material experiences in the process is very complex, the crystallization behavior is also significantly influenced by the complicated phenomena such as melting, cooling, remelting, resolidification, and annealing [8].

Continuous operation of the on-line consolidation process is achieved by rotating the mandrel during filament winding. However, the speed of on-line consolidation is limited by the quality requirements for the parts, such as bonding strength and crystallinity. In general, the winding speed, the heat intensity, and the roller pressure are used to describe the processing window of on-line consolidation. The objectives of this study were to develop process models to simulate the on-line consolidation filament winding process and identify the relationships between process variables and the structure quality. In particular, the effects of process parameters on consolidation conditions and crystallization were investigated.

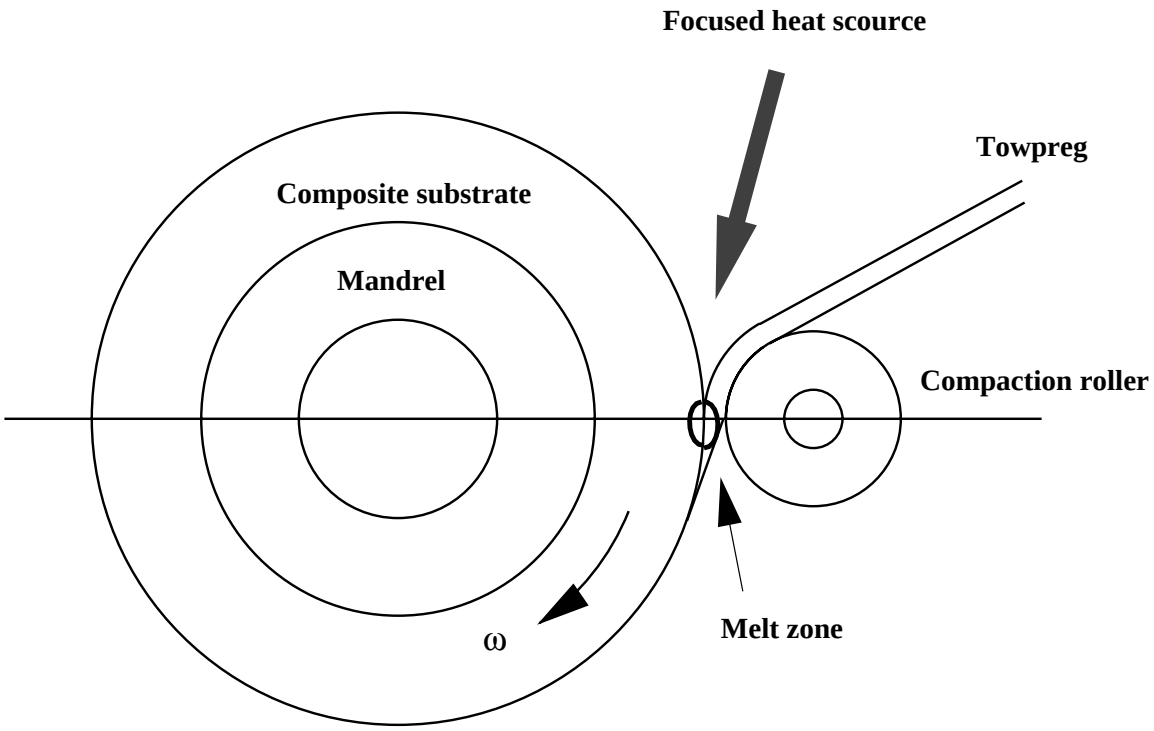

Figure 1.1 General configuration of the thermoplastic filament winding process

Chapter 2 Literature Review

Previous studies have dealt with the modeling issues involved in the on-line consolidation process of the thermoplastic composites. These include models for the heat transfer, consolidation and crystallization. A survey of the current research in these areas will be presented in this chapter.

2.1 Heat Transfer Analysis

Complicated heating and cooling cycles are involved in the manufacturing processes for thermoplastic composites. It is well known that final mechanical properties of a composite structure significantly depend on the thermal history during manufacture. A number of heat transfer models have been proposed to investigate this thermal history for tape placement [9-16] and filament winding [17-21].

Grove [11] developed a two-dimensional finite element model to investigate the temperature profile of the tape laying process with a single laser heat source. The region close to the tape/substrate interface was modeled using a coordinate system moving at the same speed as the lay up head and thus, the given geometry could be represented by a fixed finite element mesh. Furthermore, the movement of the laying head was modeled by a process of incrementally shifting the calculated temperature distribution through the mesh at an appropriate time interval.

Güceri and his coworkers [16-17] used a finite difference method to show that very high temperature gradients existed near the nip point, and that the roller velocity, heat input and preheating significantly affected the temperature field within the laminate. An Eulerian control volume, which includes the region influenced by the local heat source, was chosen and the problem was formulated as steady state using an Eulerian approach. Güceri et al. [16,17] investigated the anisotropic heat conduction phenomenon by modeling the filament wound structure as an orthotropic domain employing the concept of angle ply sublaminates. The effect of winding angle was incorporated in the effective orthotropic conductivity tensor.

James and Black [19-20] investigated the continuous filament winding process using an infrared energy source. Similar to the formulation proposed by Güceri et al., the transient thermal model was transformed into a quasi-steady problem by working in an Eulerian reference frame. The model was subdivided into two regimes. A one-dimensional Cartesian coordinate heat transfer analysis of the tape regime was coupled with a three-dimensional cylindrical coordinate heat transfer analysis of the composite/mandrel assembly. The explicit finite difference method was used to solve the problem numerically.

Shih and Loos [22] adopted the commercial finite element package, ABAQUS to study the transient heat transfer problem involved in continuous filament winding process with a hot-air heater. Assuming that little energy would propagate across the interface between compaction roller and composite substrate, the process was modeled in two parts to study the temperature profile in the substrate cylinder and the towpreg prior to reaching the nippoint, respectively. The hot-air heater was treated simply as a convective boundary condition and the hot-air film coefficient was measured by experiment. It was concluded that the hot-air heater used does not melt the resin on the surface of the substrate, but instead melts the resin of the incoming towpreg.

2.2 Nonisothermal Consolidation

The consolidation of thermoplastic composites consists of two phenomena [23]. First, two adjacent ply surfaces coalesce and come into "intimate contact" under an applied pressure. Second, bonds form at the ply interface by the autohesion process [21] in which the molecular chains diffuse across the interface and entangle with their new neighbors. The following sections discuss the previous research on intimate contact and diffusion bonding.

2.2.1 Intimate Contact

The prepreg ply surfaces are uneven and spatial gaps exist at the ply interfaces at the beginning of consolidation. Application of heat and pressure causes flow and deformation at the ply interfaces which results in intimate contact between adjacent surfaces. The degree of intimate contact is a measure of the amount of surface that is in

contact. Dara and Loos [21] used a two-parameter Weibull function to model the tow height distribution of AS4/P1700 prepregs. Lee and Springer [23] simplified the model by Dara and Loos and represented the irregular surfaces of the plies by a series of rectangular elements. Two geometric parameters, tow width and tow height, were used to describe the variations in the prepreg surface. They treated the deformation of the rectangular elements as a one-dimensional laminar squeezing flow. The geometry parameters were measured from photomicrographs of the cross section of an uncompacted ply, and the viscosity parameters were obtained by matching the model results to the degree of intimate contact versus time data.

Mantell and Springer [12] extended the Lee-Springer model [23] to incorporate the tape laying and filament winding processes. By assuming that the temperature and pressure were constant and that the contact time is equal to the arc length of contact between the roller and composite divided by the roller speed, an expression for the degree of intimate contact was derived for the tape laying process. For the filament winding process, the expression for the tape laying process is modified by replacing the roller speed with the product of the speed of mandrel rotation and the radius of the cylinder at the contact interface. To verify the model, Mantell et al. [24] conducted short beam shear tests and lap shear tests for specimens fabricated both in a press and with a specially constructed tape laying apparatus. The degree of intimate contact was determined from the C-Scan pictures by comparing the areas in contact to the total area. The model parameters were obtained by matching the model results to the degree of intimate contact versus time data.

Li and Loos [25] measured the surface roughness of the prepreg plies with a surface topology characterization machine. The prepreg geometric parameters were measured directly, and consequently, eliminate the necessity of determining the geometric parameters by matching the intimate contact data with model predictions [23,24]. Models were developed to predict the degree of intimate contact at the ply interfaces of both unidirectional and cross-ply laminates. The experimental data agreed well with the simulation results.

Sonmez and Hahn [26] used the Lee-Springer model to study on-line consolidation in the tape placement process. A heat transfer analysis was incorporated into the consolidation model to consider nonisothermal processing. Further bonding behavior during the subsequent lays up was studied. It was found that a significant portion of the bonding occurred during the placement of subsequent layers.

2.2.2 Diffusion Bonding

There have been many research investigations to study diffusion bonding of thermoplastic polymers [27-33]. Fundamental to all fusion bonding processes is the intermolecular diffusion between surfaces in intimate contact. Higher temperature promotes the diffusion process, thus shortens the required time to achieve complete bonding. Isothermal diffusion of polymer chains in an amorphous material can be modeled using the reptation and healing theories [31,32]. The diffusion behavior is characterized by a temperature dependent reptation time (T_r), which corresponds to the time needed to completely heal the interface [27-29].

Dara and Loos [21] reported the relation for autohesion of carbon fiber polysulfone composites. Dara and Loos related the temperature dependence of relaxation time to the zero shear rate viscosity and the shift factor. The temperature-dependent viscosity was represented in the form of an Arrhenius equation. By assuming that the same relation was valid for APC-2, James and Black [19] used the relation reported by Dara and Loos and examined consolidation of APC-2 plies during the filament winding process both experimentally and numerically.

Bastien and Gillespie [30] developed the nonisothermal healing model for diffusion bonding of AS4/PEEK thermoplastic composites. For nonisothermal processing, conditions commonly observed during the composites fusion bonding process, the thermal history is divided into many time intervals with sufficiently small time steps and the temperature is assumed constant over each time interval. Therefore, the isothermal healing theory can be used in each of those isothermal time steps and the nonisothermal model was developed based on the minor chain length criteria and the interpenetration distance criteria.

2.3 Crystallization

It has been shown that the mechanical properties of thermoplastic matrix composites can be related directly to the crystallinity of the polymer [34-39]. Therefore, it is essential to determine the effects of processing parameters on the crystallization behavior of the matrix to control part quality.

Most of the crystallization models used in the literature are based on the theoretical work by Avrami [40-42], Tobin [43-45] and Malkin [46,47]. Lee and Springer [23] established a model that related the cooling rate applied during processing to the crystallinity of the material. The model was developed for a flat plate in which the temperature varied only across the plate but not along the plate. The simple expression proposed by Ozawa [48] was adopted to correlate the measured rate of crystallization with temperature. The heat transfer analysis to study the temperature distribution and the crystallization model were coupled by taking heat generated due to crystallization into account in the energy equation. A finite element algorithm was developed to calculate the temperature and the crystallinity as functions of position and time. The model was verified by the tests to measure the crystallinity of PEEK 150P polymer specimens cooled at different rates. The cooling rates were determined by recording the temperature inside APC-2 composites during cooling. The crystallinities of the specimens were measured by differential scanning calorimetry (DSC).

Mantell and Springer [12] studied the crystallization behavior in the tape placement process. The rate of change in crystallinity was related to the crystallinity, the temperature and the change in temperature by several empirical expressions [23,49-51]. During heating, the model proposed by Maffezzoli et al. [49] was adopted. During cooling, the model of Lee and Springer [23] or the model developed by Velisaris and Seferis [50,51] was applied. Nejhad et al. [52] applied the Velisaris and Seferis model [50,51] to the filament winding process.

Choe and Lee [53] developed a kinetic model for the nonisothermal crystallization of PEEK based on Tobin Equation [43-45]. Development of a crystalline phase in the PEEK polymer melt includes two competing nucleation and growth processes, heterogeneous nucleation and homogeneous nucleation. The crystallization

kinetics was expressed in terms of a linear combination of two Tobin expressions. The model included the effect of melt temperature and correlated well with nonisothermal crystallization data. Sonmez and Hahn [8] used the Choe and Lee model [53] to study the crystallization in tape placement process.

Chapter 3 Heat Transfer Analysis

3.1 Introduction

During processing, thermoplastic composites undergo a number of microstructural changes such as melting, crystallization, and autohesion depending on the thermal history. Hence, the resulting material properties depend strongly on their thermal history. Therefore, it is important to control the temperature distribution inside the composite during consolidation to ensure the quality of the fabricated part. A comprehensive thermal analysis must be developed to predict the complex temperature changes that occur inside the composite during the manufacturing process.

In the on-line thermoplastic filament winding process, a high-intensity heat source is focused at the interface between incoming towpreg and the composite substrate, and a molten region is formed at the nippoint. (Figure 3.1) There are four components included in the domain of interest: the composite substrate, mandrel, towpreg, and compaction roller.

Note that the heat source is aimed at the surfaces of both the towpreg and the composite substrate simultaneously. We assumed that little energy would propagate across the interface between the roller and composite cylinder. Hence, the analysis was divided into two parts: the composite-mandrel assembly and the towpreg-roller assembly.

In the present investigation, the hot air heater uniformly heats the substrate cylinder along the mandrel axial direction and the towpreg across the width, so the heat conduction problem is reduced to separate 2-D finite element heat transfer models for the composite substrate and the towpreg. The analysis was performed using an Eulerian approach. In a previous experimental study by Shih and Loos [22], it was concluded that the hot-air heater does not heat the surface of the substrate up to the melt temperature of the matrix resin, but a melt region is formed on the surface of the incoming towpreg in the nippoint.

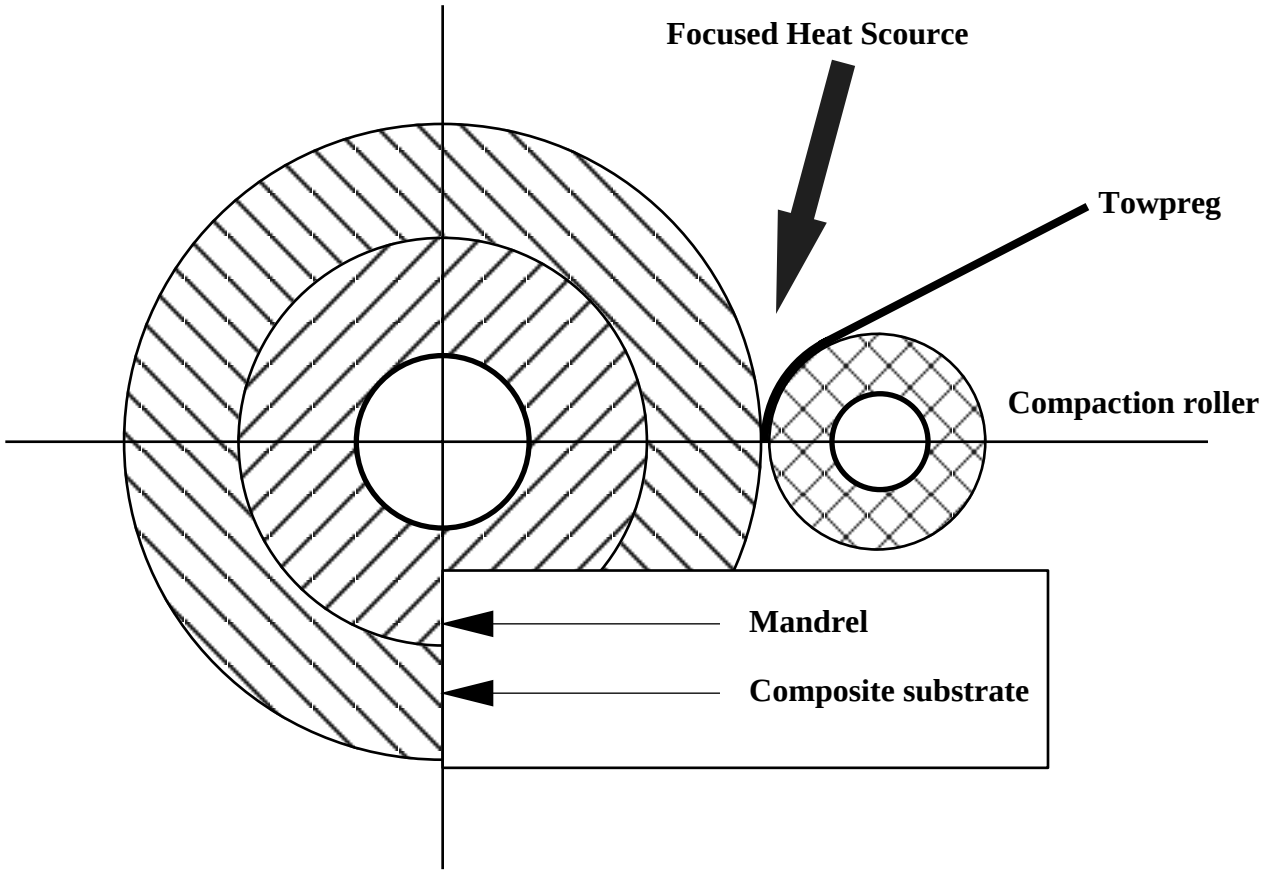

Figure 3.1 Geometry of the heat transfer problem

3.2 Simulation on Heating of the Substrate Cylinder

Figure 3.2 displays the control volume, the boundaries, and the coordinate system used in simulation on heating of the substrate cylinder. The composite-mandrel assembly is rotated at a certain speed. In order to simulate the mandrel rotation, the coordinate system is fixed onto the hot-air heater and we move the hot-air heater in the opposite direction of the mandrel rotation instead. The thickness of the towpreg is small and the increase in the diameter of the composite substrate in one rotation is negligible. A quasi-steady state is assumed to prevail throughout the process and the problem is formulated as steady state in the Eulerian framework.

3.2.1 Governing Equation

By applying the principle of conservation of energy to a finite differential region, the temperature distribution of the composite-mandrel assembly is governed by the conductive heat transfer equation given as,

$$\rho c_p \dot{T} = \dot{Q} + \nabla \cdot (\tilde{k} \cdot \nabla T) \tag{3.1}$$

where ρ is the density, C_p is the specific heat capacity, $\tilde{k}$ is thermal conductivity tensors, T is temperature, t is time and $\dot{T} = \frac{DT}{Dt}$. The left hand side of the equation, $\rho C_p \dot{T}$, represents the rate of change of thermal energy stored within the control volume. The first term on the right hand side of the equation, $\dot{Q}$, is the volumetric rate of thermal energy generation, and the second term, $\nabla \cdot (\tilde{k} \cdot \nabla T)$, represents the net conduction heat rate into a unit volume.

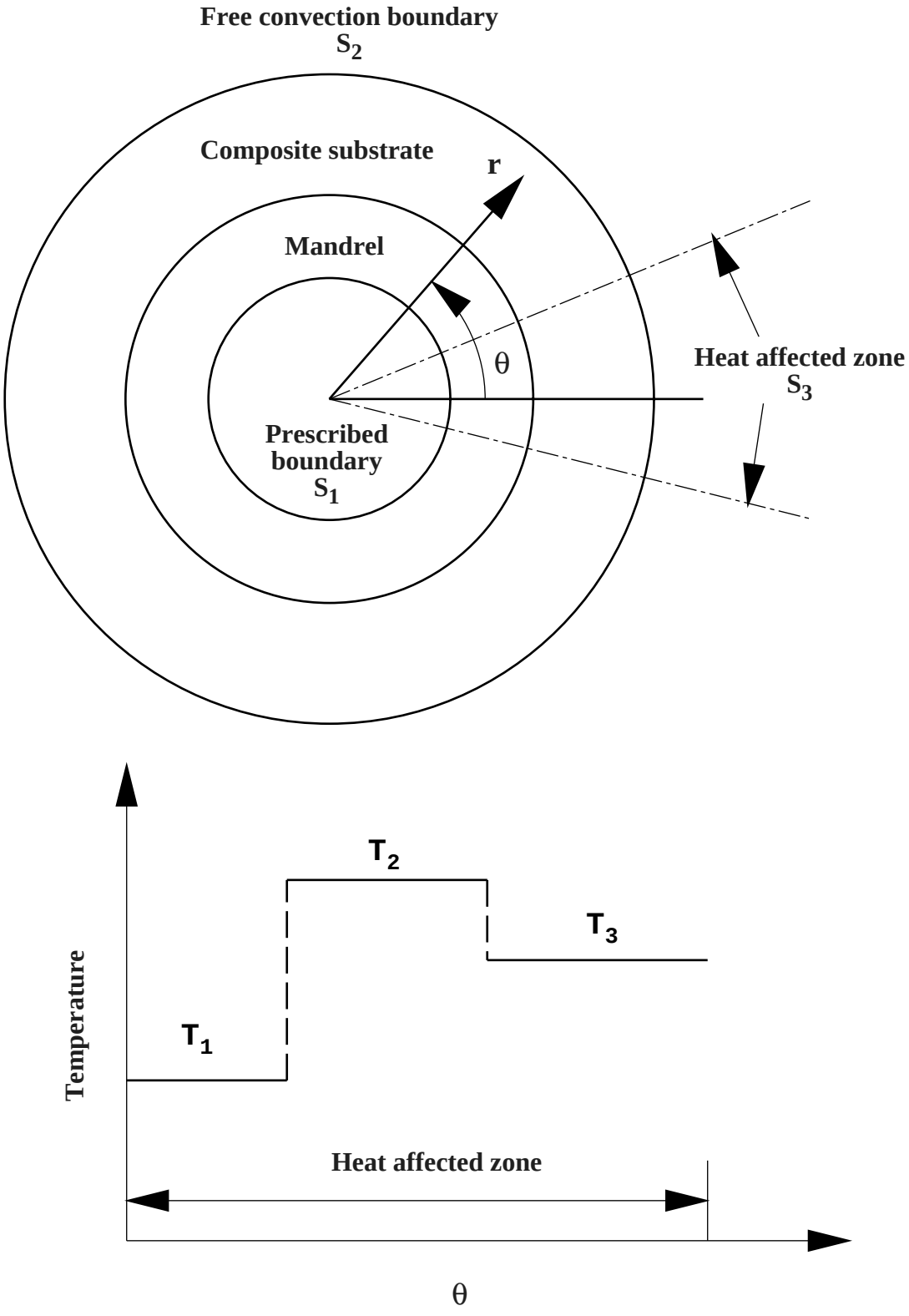

Figure 3.2 The control volume and boundary conditions of the winding problem

In the domain of interest, the composite is heterogeneous with the fiber and matrix having different thermophysical properties and the mandrel is generally isotropic and homogeneous. In order to simplify the analysis, we treat the composite as an anisotropic yet homogeneous continuum.

The composite tow is assumed to be a transversely isotropic (in the plane normal to the fiber direction) material. k_L and k_T are the tow principal conductivities in the longitudinal and transverse directions, respectively. k_L and k_T are assumed to be constant. The anisotropy of the composite substrate is modeled as an orthotropic domain employing the concept of angle ply sublaminates [16,17]. Therefore the effective orthotropic conductivity tensor is

$$\tilde{k} = \begin{bmatrix} k_r & 0 \\ 0 & k_\theta \end{bmatrix} \tag{3.2}$$

where k_r is the conductivity in the radial direction and is equivalent to k_T, k_θ is the conductivity in the circumferential direction expressed as

$$k_\theta = k_T \cos^2 \phi + k_L \sin^2 \phi \tag{3.3}$$

where ϕ is the winding angle.

In comparison to the amount of heat supplied to melt the resin in the towpreg material, the heat generation due to crystallization, $\dot{Q}$, is negligible for the composite substrate and the term does not apply to the mandrel.

Therefore, in a fixed coordinate system, (R,Θ), the governing energy equation becomes

$$\rho C_p \frac{DT}{Dt} = \frac{1}{R} k_R \frac{\partial}{\partial R}(R \frac{\partial T}{\partial R}) + \frac{1}{R} k_\Theta \frac{\partial}{\partial \Theta}(\frac{1}{R} \frac{\partial T}{\partial \Theta}) \tag{3.4}$$

The heat source is moving along the circumferential direction and the relation between fixed coordinate system (R,Θ) and the moving one (r,θ) is as follows:

$$R = r$$
$$\Theta = \theta - \omega t \tag{3.5}$$

where ω is the mandrel winding speed.

Consequently,

$$\frac{\partial \theta}{\partial t} = \omega$$
$$\frac{\partial R}{\partial t} = 0 \tag{3.6}$$

When using the Eulerian description, the variables are expressed in terms of instantaneous position and time, and the comoving derivative of local temperature T is given as,

$$\frac{DT(R,\Theta,t)}{Dt} = \frac{\partial T(r,\theta,t)}{\partial t} + (\frac{\partial T(r,\theta,t)}{\partial r}\frac{\partial r}{\partial t} + \frac{\partial T(r,\theta,t)}{\partial \theta}\frac{\partial \theta}{\partial t}) \tag{3.7}$$

Combining equation (3.6) and equation (3.7),

$$\frac{DT(R,\Theta,t)}{Dt} = \frac{\partial T}{\partial t} + \omega \frac{\partial T}{\partial \theta} \tag{3.8}$$

With the steady-state assumption, the first term on the right hand side of equation (3.8) vanishes and the governing equation is given in equation (3.9).

$$\rho C_p \omega \frac{\partial T}{\partial \theta} = \frac{1}{r} k_r \frac{\partial}{\partial r}(r \frac{\partial T}{\partial r}) + \frac{1}{r} k_\theta \frac{\partial}{\partial \theta}(\frac{1}{r}\frac{\partial T}{\partial \theta}) \tag{3.9}$$

3.2.2 Boundary Conditions

For the inner surface of the mandrel, that is, the boundary S_1 in Figure 3.2, the temperature is prescribed to be a constant. If the mandrel is preheated, it is equal to the preheat temperature:

$$T = T_i \quad on \quad S_1 \tag{3.10}$$

For S_2, the area exposed to air, we have the free convection boundary condition:

$$k_r \frac{\partial T}{\partial r} = -h_a (T - T_a) \quad on \quad S_2 \tag{3.11}$$

where h_a is the film coefficient and T_a is the air temperature.

A hot gas torch is used to heat the interface between the composite substrate and the towpreg. In the heat affected zone, the following forced convection boundary condition is prescribed:

$$k_r \frac{\partial T}{\partial r} = -h_{hg} (T - T_{hg}) \quad on \quad S_3 \tag{3.12}$$

where h_{hg} is the hot gas film coefficient and T_{hg} is the temperature of the hot gas.

In previous experimental work by Shih and Loos [22], it was noted that the hot gas temperature in the heat-affected zone is not uniform and the highest temperature occurs around the nippoint. Therefore a series of step functions as shown in Figure 3.2 are used to model the temperature variation in the heat-affected zone.

3.2.3 Sector Element

In the present study, a four-node 'sector element' in polar coordinates is used to discretize the domain of interest.

As shown in Figure 3.3, the sector element is formed by two straight sides with θ constant and two arcs with r constant. The domain of a sector element is defined by the locations of its four nodal points $\tilde{r}_a, a = 1, \cdots, 4$ in the $\boldsymbol{R}^2$ plane. We assume the nodal points are labeled in ascending order corresponding to the counterclockwise direction (see Figure 3.3). We seek a change of coordinates which maps the given sector into the biunit square called the parent domain, as depicted in Figure 3.4. The coordinates of a point $\tilde{\xi} = \begin{Bmatrix} \xi \\ \eta \end{Bmatrix}$ in the Biunit Square are to be related to the coordinates of a point $\tilde{r} = \begin{Bmatrix} r \\ \theta \end{Bmatrix}$ in Ω^e by mappings of the form

$$
\begin{aligned}
r &= \frac{r_2 - r_1}{2}\xi + \frac{r_2 + r_1}{2} \\
\theta &= \frac{\theta_2 - \theta_1}{2}\eta + \frac{\theta_2 + \theta_1}{2}
\end{aligned}
\tag{3.13}
$$

The shape functions in the parent domain are

$$
\begin{aligned}
N_1 &= (1-\xi)(1-\eta)/4 \\
N_2 &= (1+\xi)(1-\eta)/4 \\
N_3 &= (1+\xi)(1+\eta)/4 \\
N_4 &= (1-\xi)(1+\eta)/4
\end{aligned}
\tag{3.14}
$$

The definition of a sector element facilitates the finite element formulation of the problems in the polar coordinate system. Sector elements give a better representation of the curved boundary shape which should require fewer element to achieve the same solution accuracy as rectangle or triangle elements in the Cartesian-coordinate system.

3.2.4 Finite Element Formulation

With the governing equation and boundary conditions specified, the statement of the problem is:

Determine $T(r,\theta)$ such that

$$
\begin{aligned}
&\frac{1}{r}k_r\frac{\partial}{\partial r}\left(r\frac{\partial T}{\partial r}\right) + \frac{1}{r}k_\theta\frac{\partial}{\partial \theta}\left(\frac{1}{r}\frac{\partial T}{\partial \theta}\right) = \rho c\omega\frac{\partial T}{\partial \theta} && in \quad \Omega \\
&T = T_i && on \quad S_1 \\
&-k_r\frac{\partial T}{\partial r} = h_a(T - T_a) && on \quad S_2 \\
&-k_r\frac{\partial T}{\partial r} = h_{hg}(T - T_{hg}) && on \quad S_3
\end{aligned}
\tag{3.15}
$$

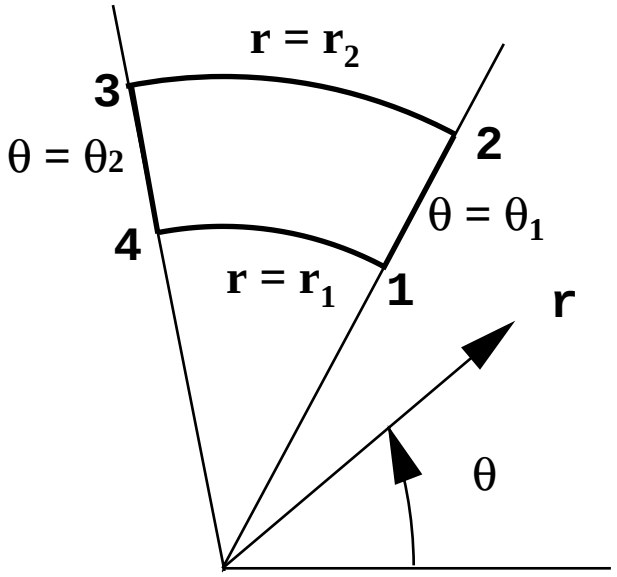

Figure 3.3 Four−node sector element

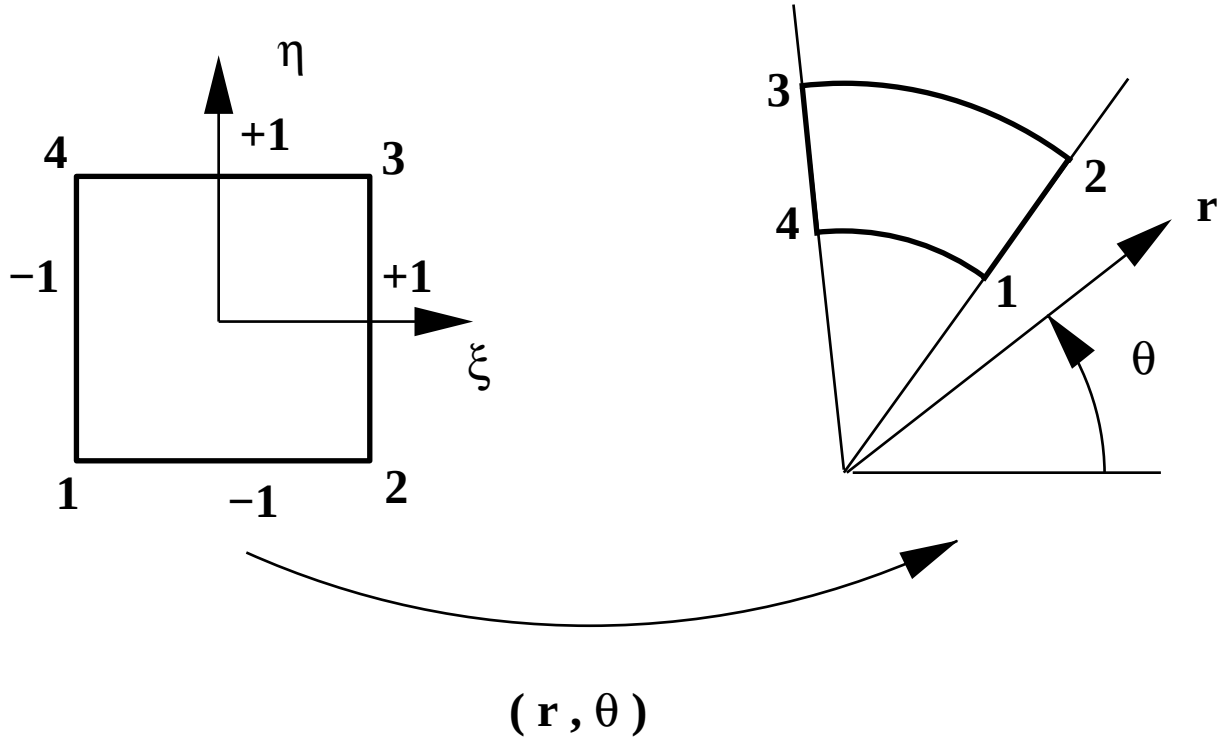

Figure 3.4 Mapping of parent domain and local element domain

Galerkin's method [54] is used to derive a finite element formulation. We elaborate upon this below:

Let $\phi : \overline{\Omega} \to R$ be a smooth function such that $\phi = 0$ on S_1, that is, ϕ vanishes on the part of the boundary where essential boundary conditions are prescribed.

Multiplying both sides of the governing eq. (3.15) by ϕ and integrating the result over the domain Ω we obtain

$$\iint_{\Omega} \phi \left[\frac{1}{r} k_r \frac{\partial}{\partial r}(r \frac{\partial T}{\partial r}) + \frac{1}{r} k_\theta \frac{\partial}{\partial \theta}(\frac{1}{r} \frac{\partial T}{\partial \theta}) - \rho c \omega \frac{\partial T}{\partial \theta} \right] r dr d\theta = 0 \tag{3.16}$$

By using the chain rule of differentiation, we get

$$\begin{aligned} \iint_{\Omega} \phi \frac{1}{r} k_r \frac{\partial}{\partial r}(r \frac{\partial T}{\partial r}) r dr d\theta &= \iint_{\Omega} k_r \left[\frac{\partial}{\partial r}(\phi r \frac{\partial T}{\partial r}) - r \frac{\partial \phi}{\partial r} \frac{\partial T}{\partial r} \right] dr d\theta \\ \iint_{\Omega} \phi \frac{1}{r} k_\theta \frac{\partial}{\partial \theta}(\frac{1}{r} \frac{\partial T}{\partial \theta}) r dr d\theta &= \iint_{\Omega} k_\theta \left[\frac{\partial}{\partial \theta}(\frac{\phi}{r} \frac{\partial T}{\partial \theta}) - \frac{1}{r} \frac{\partial \phi}{\partial \theta} \frac{\partial T}{\partial \theta} \right] dr d\theta \end{aligned} \tag{3.17}$$

The use of the Gauss's theorem yields

$$\begin{aligned} \iint_{\Omega} k_r \frac{\partial}{\partial r}(\phi r \frac{\partial T}{\partial r}) dr d\theta &= \int_S k_r \phi r \frac{\partial T}{\partial r} n_r ds \\ \iint_{\Omega} k_\theta \frac{\partial}{\partial \theta}(\frac{\phi}{r} \frac{\partial T}{\partial \theta}) dr d\theta &= \int_S k_\theta \frac{\phi}{r} \frac{\partial T}{\partial \theta} n_\theta ds \end{aligned} \tag{3.18}$$

Substitution from eq. (3.18) into eq. (3.17) and the result into eq. (3.16) yields

$$\begin{aligned} &\iint_{\Omega} (k_r \frac{\partial \phi}{\partial r} \frac{\partial T}{\partial r} + k_\theta \frac{1}{r^2} \frac{\partial \phi}{\partial \theta} \frac{\partial T}{\partial \theta} + \phi \rho c \omega \frac{\partial T}{\partial \theta}) r dr d\theta \\ &- \int_S \phi (k_r r \frac{\partial T}{\partial r} n_r + k_\theta \frac{1}{r} \frac{\partial T}{\partial \theta} n_\theta) ds = 0 \end{aligned} \tag{3.19}$$

The last term of the above equation vanishes on the boundary S_1, where ϕ is 0. On the boundaries S_2 and S_3:

$$\begin{aligned} &n_r ds = d\theta \\ &n_\theta = 0 \\ &r = r_o \end{aligned} \tag{3.20}$$

where r_o is the outer surface radius of the substrate cylinder.

The last term on the right-hand side of eq. (3.19) satisfies convection boundary conditions given in eq. (3.15), and eq. (3.19) becomes

$$\begin{aligned}&\iint_\Omega (k_r \frac{\partial \phi}{\partial r}\frac{\partial T}{\partial r} + k_\theta \frac{1}{r^2}\frac{\partial \phi}{\partial \theta}\frac{\partial T}{\partial \theta} + \phi\rho\, c\omega \frac{\partial T}{\partial \theta}) r dr d\theta \\ &+ \int_{S_2} h_a r_o \phi\, T d\theta + \int_{S_3} h_{hg} r_o \phi\, T d\theta = \int_{S_2} h_a r_o \phi\, T_a d\theta + \int_{S_3} h_{hg} r_o \phi\, T_{hg} d\theta\end{aligned} \tag{3.21}$$

With the definitions

$$\begin{aligned}B(\phi, T) = &\iint_\Omega (k_r \frac{\partial \phi}{\partial r}\frac{\partial T}{\partial r} + k_\theta \frac{1}{r^2}\frac{\partial \phi}{\partial \theta}\frac{\partial T}{\partial \theta} + \phi\rho\, c\omega \frac{\partial T}{\partial \theta}) r dr d\theta \\ &+ \int_{S_2} h_a r_o \phi\, T d\theta + \int_{S_3} h_{hg} r_o \phi\, T d\theta\end{aligned} \tag{3.22}$$

and

$$l(\phi) = \int_{S_2} h_a r_o T_a \phi\, d\theta + \int_{S_3} h_{hg} r_o T_{hg} \phi\, d\theta \tag{3.23}$$

we can write eq. (3.21) as

$$B(\phi, T) = l(\phi) \tag{3.24}$$

Let

$$H^1 = \{\psi \mid \psi : \overline{\Omega} \to R, \int_\Omega \nabla\psi . \nabla\psi\, d\Omega < \infty\} \tag{3.25}$$

$$H_0^1 = \{\psi \in H^1, \psi = 0 \text{ on } S_1\} \tag{3.26}$$

we can now state the weak form, W, of the given problem as follows. W: Find $T \in H^1$ such that $T = T_i$ *on* S_1 and equation (3.24) holds for every $\phi \in H_0^1$.

In order to derive the Galerkin formulation of the problem, we introduce an auxiliary function $G \in H^1$ such that $G = T_i$ *on* S_1. Then for every $F \in H_0^1$, $F + G \in H^1$. Substitution of $T = F + G$ in eq. (3.24) yields

$$B(\phi, F) = l(\phi) - B(\phi, G) \tag{3.27}$$

Thus, the Galerkin formulation of the given boundary-value problem can be stated as follows: Find $F \in H_0^1$ such that eq. (3.27) holds $\forall \phi \in H_0^1$. Let H_0^{1n} be a finite dimensional subset of H_0^1 and $F^n \in H_0^{1n}$, $\phi^n \in H_0^{1n}$. Then the Galerkin approximation of the given problem is:

Find $F^n \in H_0^{1n}$ such that

$$B(\phi^n, F^n) = l(\phi^n) - B(\phi^n, G) \tag{3.28}$$

for every $\phi^n \in H_0^{1n}$.

Let $\psi_1, \psi_2, \cdots, \psi_n$ denote a set of basis functions in H_0^{1n}. Then we can write

$$\phi^n = c_i \psi_i, \quad F^n = d_j \psi_j \tag{3.29}$$

where summation on a repeated index is implied and the indices i and j range over 1 through n. The linearity of $B(\cdot,\cdot)$ in each of its arguments implies that

$$B(\phi^n, F^n) = B(c_i \psi_i, d_j \psi_j) = c_i B(\psi_i, \psi_j) d_j = c_i K_{ij} d_j \tag{3.30}$$

where

$$K_{ij} = B(\psi_i, \psi_j) \tag{3.31}$$

Similarly, with $P_i = l(\psi_i)$,

$$l(\phi^n) = l(c_i \psi_i) = c_i l(\psi_i) = c_i P_i \tag{3.32}$$

Eq. (3.28) becomes

$$c_i K_{ij} d_j = c_i (P_i - B(\psi_i, G)) . \tag{3.33}$$

Since eq. (3.28) holds for every ϕ^n, therefore eq. (3.33) should hold for every choice of $c_1, c_2, \cdots, c_n$, which is possible if and only if

$$K_{ij} d_j = P_i - B(\psi_i, G), \qquad i = 1,2,\cdots,n \tag{3.34}$$

The matrices K and P are called the global stiffness matrix and load vector, respectively.

In practice, the global stiffness matrix and load vector are assembled element by element for the entire mesh by ignoring the contributions to the load vector from terms containing the function G. Essential boundary condition $T = T_i \ on \ S_1$ is imposed by the standard procedure to modify the global stiffness matrix and load vector. The algebraic equations are solved to get the nodal temperatures.

Basis Functions can be obtained by patching together the appropriate shape functions. In the present study, four-node sector elements introduced in Section 3.2.3 are used. We assume a suitable variation of temperature in a finite element as

$$T^n(r,\theta) = \sum_{i=1}^{4} N_i(r,\theta) d_i \tag{3.35}$$

where N_i are shape functions.

The global stiffness matrix and load vector can be assembled with the element stiffness matrices and load vectors.

$$\begin{aligned} [K_{ij}] &= \sum [K_{mn}]^e \qquad && m,n = 1,2,\cdots,4 \\ [P_i] &= \sum [P_m]^e \qquad && i,j = 1,2,\cdots,n \end{aligned} \tag{3.36}$$

where

$$\begin{aligned} K_{mn}{}^e &= K_{mn}{}' + K_{mn}{}'' + K_{mn}{}''' \\ P_m{}^e &= \int_{S_2 \cap \Omega^e} h_a T_a r_o N_m d\theta + \int_{S_3 \cap \Omega^e} h_{hg} T_{hg} r_o N_m d\theta \\ K_{mn}{}' &= \iint_{\Omega^e} (k_r \frac{\partial N_m}{\partial r} \frac{\partial N_n}{\partial r} + k_\theta \frac{1}{r^2} \frac{\partial N_m}{\partial \theta} \frac{\partial N_n}{\partial \theta}) r dr d\theta \\ K_{mn}{}'' &= \iint_{\Omega^e} (\rho c \omega N_m \frac{\partial N_n}{\partial \theta}) r dr d\theta \\ K_{mn}{}''' &= \int_{S_2 \cap \Omega^e} h_a r_o N_m N_n d\theta + \int_{S_3 \cap \Omega^e} h_{hg} r_o N_m N_n d\theta \end{aligned} \tag{3.37}$$

By using the mappings of the form shown in eq. (3.13), eq. (3.37) can be integrated in the parent domain (ξ, η):

$$
\begin{aligned}
P_m^{\ e} &= h_a T_a r_o \int_{-1}^{1} \left(\frac{d\theta}{d\eta} N_m\right)_{S_2 \cap \Omega^e} d\eta + h_{hg} T_{hg} r_o \int_{-1}^{1} \left(\frac{d\theta}{d\eta} N_m\right)_{S_3 \cap \Omega^e} d\eta \\
K_{mn}^{\ '} &= \int_{-1}^{1}\int_{-1}^{1} \left[k_r r \frac{\partial N_m}{\partial \xi}\frac{\partial N_n}{\partial \xi}\left(\frac{d\xi}{dr}\right)^2 + k_\theta \frac{1}{r}\frac{\partial N_m}{\partial \eta}\frac{\partial N_n}{\partial \eta}\left(\frac{d\eta}{d\theta}\right)^2\right]\frac{dr}{d\xi}\frac{d\theta}{d\eta} d\xi\, d\eta \\
K_{mn}^{\ ''} &= \int_{-1}^{1}\int_{-1}^{1} \left[\rho c \omega r N_m \frac{\partial N_n}{\partial \eta}\frac{d\eta}{d\theta}\right]\frac{dr}{d\xi}\frac{d\theta}{d\eta} d\xi\, d\eta \\
K_{mn}^{\ '''} &= h_a r_o \int_{-1}^{1} \left(\frac{d\theta}{d\eta} N_m N_n\right)_{S_2 \cap \Omega^e} d\eta + h_{hg} r_o \int_{-1}^{1} \left(\frac{d\theta}{d\eta} N_m N_n\right)_{S_3 \cap \Omega^e} d\eta
\end{aligned}
\tag{3.38}
$$

3.2.5 Accuracy Evaluation

In order to evaluate the accuracy of the finite element code, we study a problem with a known analytical solution and compare the numerical solution to the analytical solution. In the polar coordinate system (r,θ), consider an infinitely long cylinder with the inner and outer radii of R_i and R_o, respectively. The surface temperatures are specified. Two cases with different surface temperature distribution are tested.

In the first case, the temperature on the inner surface, T_{inner} is $50^o C$ and the temperature on the outer surface, T_{outer} is $100^o C$. The temperature at any distance r from the center is expressed as [55]

$$
T = T_{outer} + \frac{\Delta T}{\ln(r_o / r_i)} \ln(r_o / r) \tag{3.39}
$$

where $\Delta T = T_{inner} - T_{outer}$.

In the second case, the temperature on the upper half outer surface, T_{outer_u} is $100^o C$, the temperature on the lower half outer surface, T_{outer_l} is $0^o C$, and the temperature on the inner surface, T_{inner} is the average of T_{outer_u} *and* T_{outer_l}, that is, $50^o C$. The temperature at any point (r,θ) in the cylinder is [55]

$$
T(r,\theta) = T_{inner} + \sum_{n=1,3,5,\cdots}^{\infty} \frac{2(T_{outer_u} - T_{outer_l})}{n\pi}\left(\frac{r}{r_o}\right)^n \frac{r^{-2n} - r_i^{-2n}}{r_o^{-2n} - r_i^{-2n}} \sin(n\theta) \tag{3.40}
$$

As shown in Figures 3.5, 3.6 and 3.7, the temperature simulations compared well.

3.2.6 Results

Shih and Loos [22] measured temperature profiles in a composite ring during the winding process. The on-line consolidation, filament winding system included a computer-controlled filament winding machine and a consolidation head which housed a compaction roller and a hot-air heater. In order to measure the temperature profile during the winding and consolidation processes, a 26-ply APC-2 thermoplastic composite ring was manufactured with eight K-type, fast responding thermocouples installed in various positions inside the ring. The position of each thermocouple is shown in Figure 3.8. The thermocouples captured the local temperature history.

The finite element model presented in Section 3.2.4 and Section 3.2.5 was used to calculate the temperature distribution in the composite ring during winding. Figure 3.9 shows the finite element mesh used in the simulation. Through the thickness, the five inner most elements are assigned for the aluminum mandrel and one element is assigned for each layer of towpreg wound. There are 3000 four node sector elements used in this simulation with finer mesh in heat affected zone. Table 3.1 shows the input material property parameters for the heat transfer calculations. The properties of APC-2, carbon fiber PEEK matrix towpreg were used for the composite ring. The towpregs were wound onto an aluminum mandrel with the inner radius of 66.80 mm and outer radius of 73.05mm. The boundary condition parameters used for the calculations are listed in Table 3.2.

Note, the formula to relate the fixed coordinate system (R,Θ) in Lagrangian framework to the moving one (r,θ) in Eulerian framework is $\Theta = \theta - \omega t$. The relationship yields

$$t = \frac{\theta - \Theta}{\omega} \tag{3.41}$$

Using eq. (3.41), the resulting temperature distribution $T(r,\theta)$ in Eulerian framework is transformed into temperature history $T(R,\Theta,t)$ in Lagrangian framework. The temperature data from thermocouples denoted as Tc0, Tc1, Tc2, Tc7 were compared with the numerical predictions for different winding speeds of 1rpm, 1.5rpm and 2rpm in

Figures 3.10, 3.11, and 3.12, respectively. Very high temperature gradients are observed around the nippoint. The predictions for the temperature between the 22nd and 23rd layers were about 10% higher than the measured temperatures. Nevertheless the overall prediction captured the transient heating very well. The mandrel speed significantly affected the temperature field within the composite cylinder. The predicted temperatures for the outermost layer, layer 26, are compared for winding speeds of 1.0rpm, 1.5rpm and 2.0rpm in Figure 3.13. As expected, higher winding speed yields lower surface temperature. It should be noted that the maximum temperature on the surface of the composite cylinder is well below the melting temperature of PEEK resin composite. The simulation confirms the experimental observation that it may be difficult to create a molten zone on the surface of substrate cylinder for the processing conditions studied. In order to successfully consolidate the thermoplastic composites using the on-line consolidation technique, the air heater must focus on melting the resin in the incoming towpreg. A finite element model is constructed to predict the temperature distribution in the towpreg in the following sections.

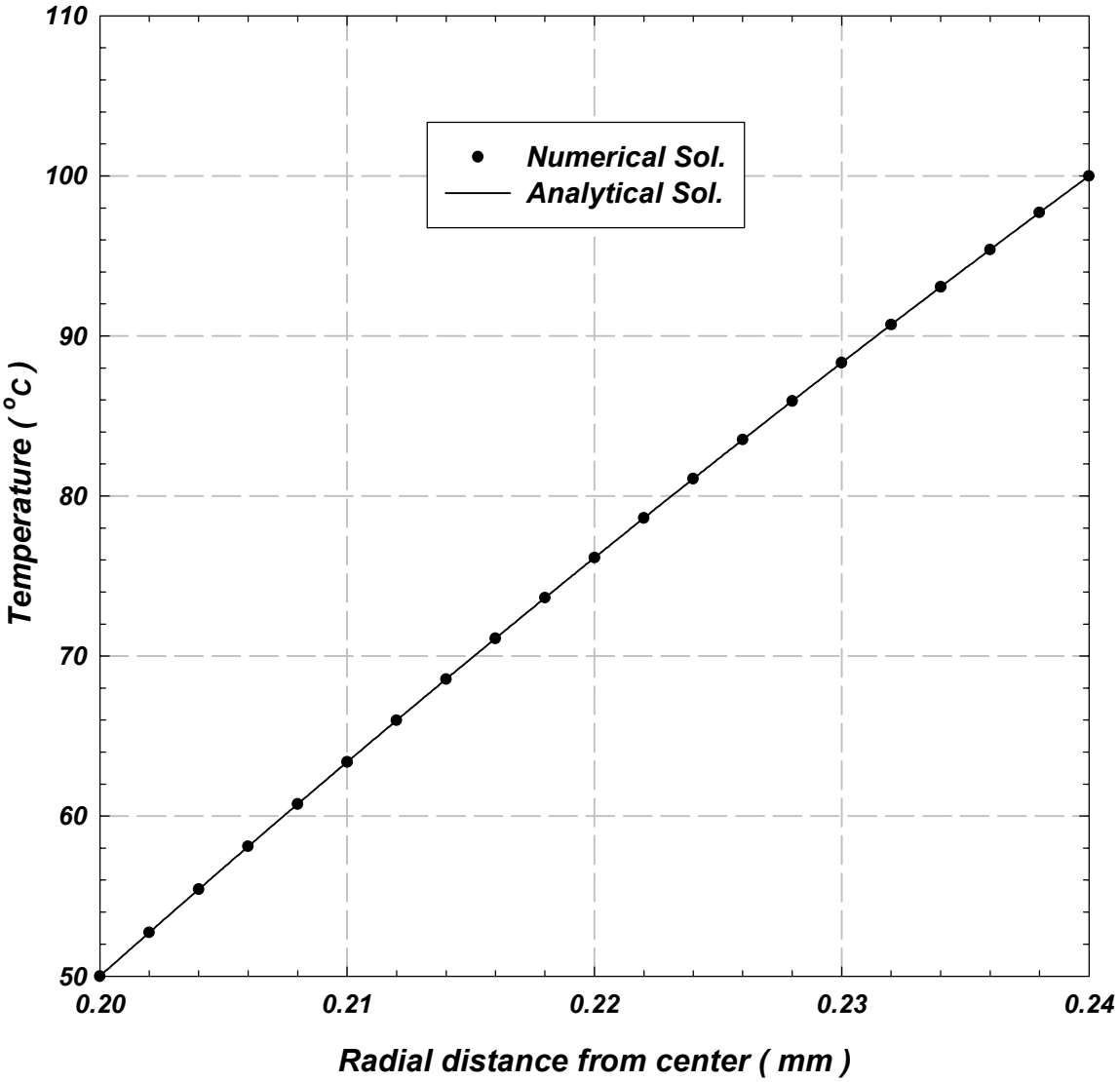

Figure 3.5 Temperature as a function of radial distance from center for hollow isotropic cylinder. Comparison between the finite element solution and analytical solution (Eqn 3.39)

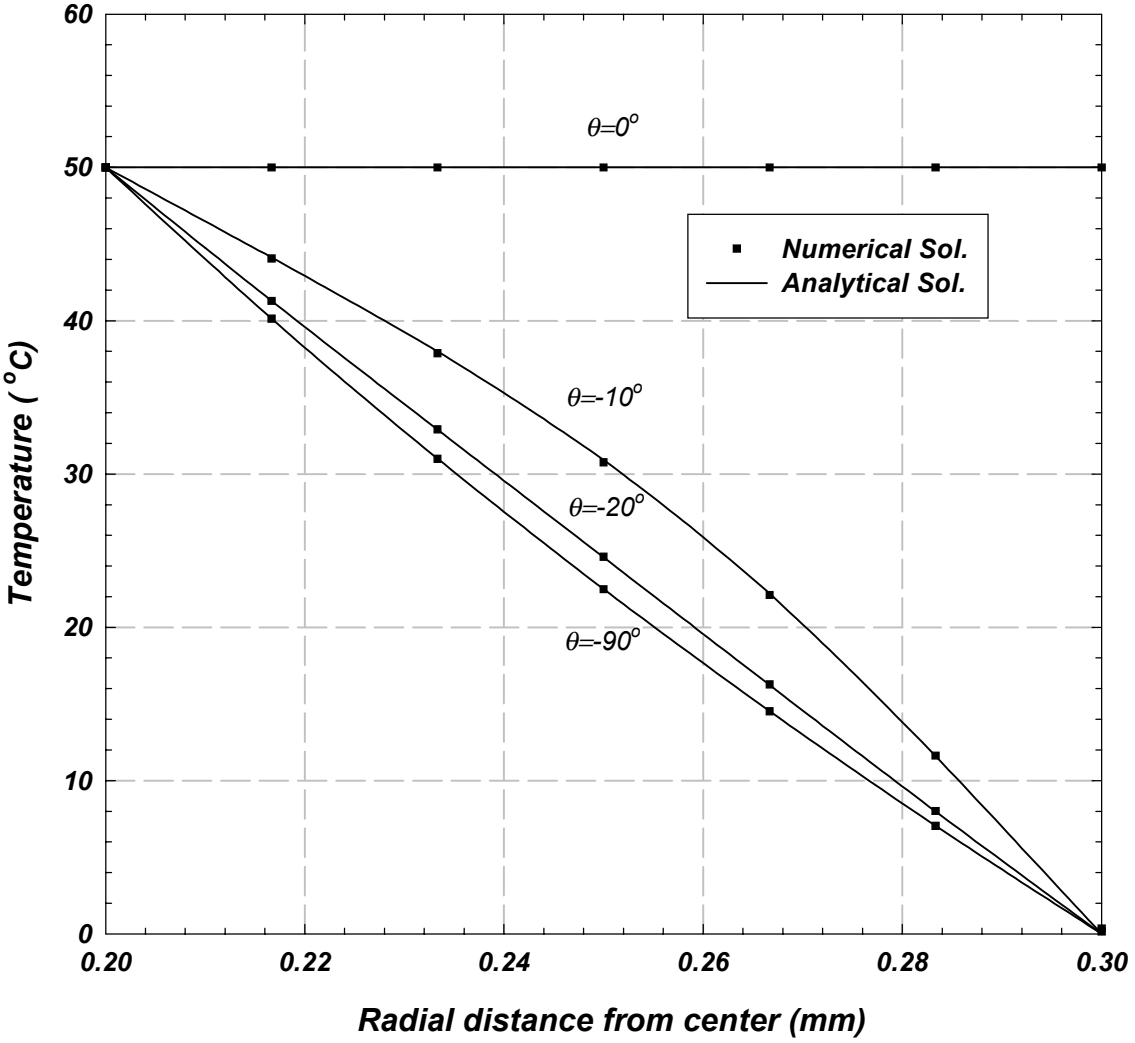

Figure 3.6 Temperature distribution in the lower half of isotropic hollow cylinder. Comparison between the finite element solution and analytical solution (Eqn 3.40)

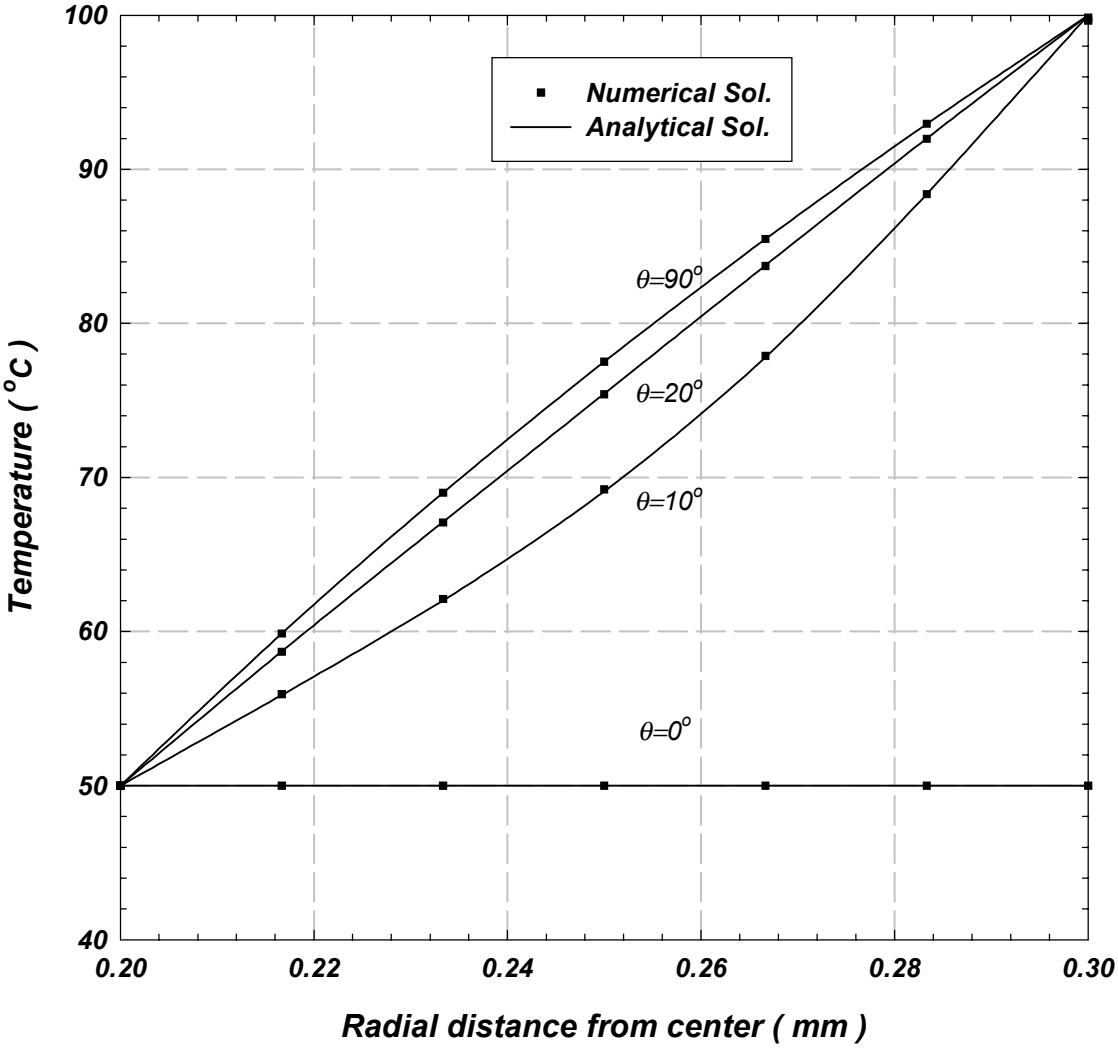

Figure 3.7 Temperature distribution in the upper half of isotropic cylinder. Comparison between the finite element solution and analytical solution (Eqn 3.40)

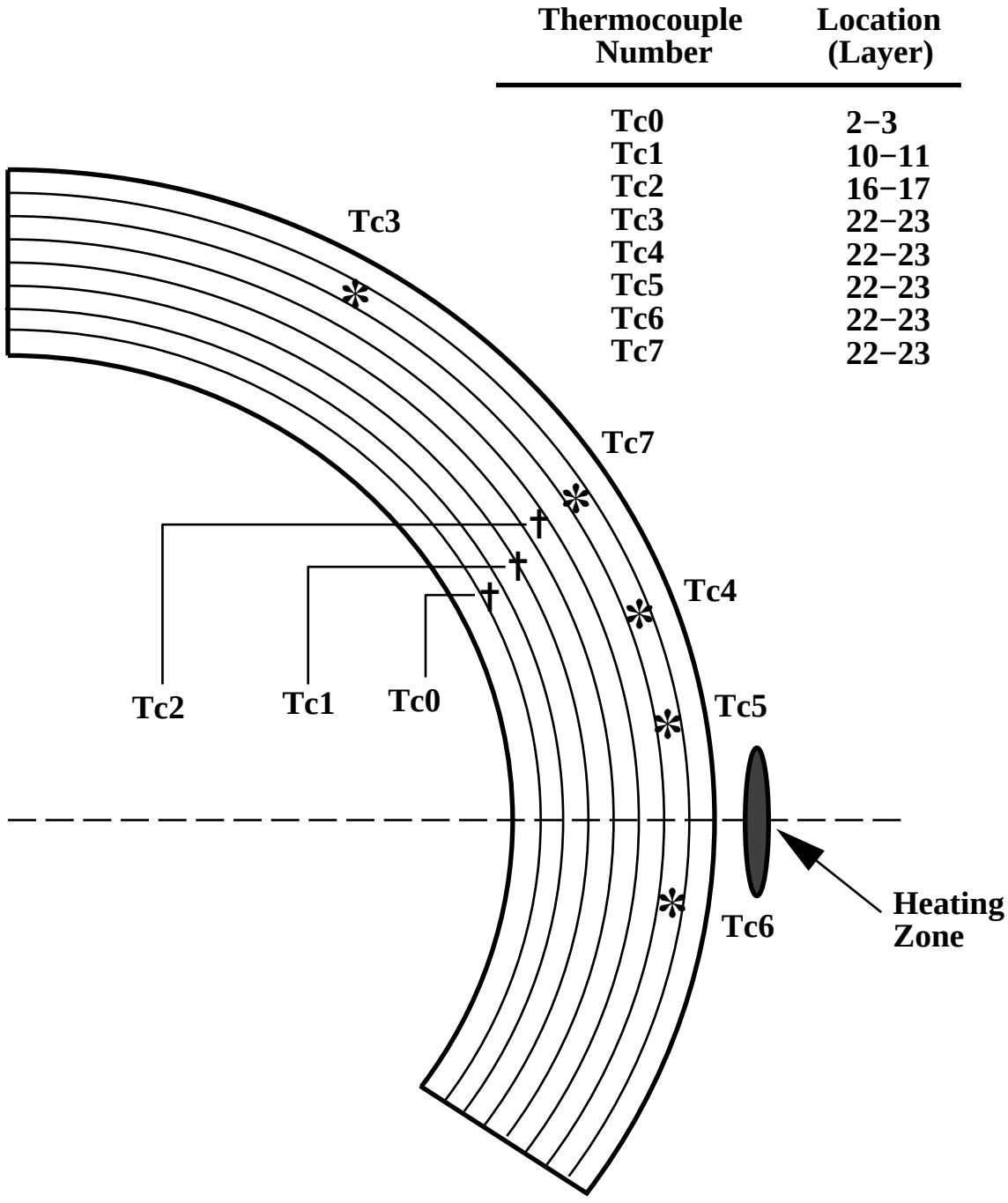

Figure 3.8 Locations of thermocouples installed in the composite ring

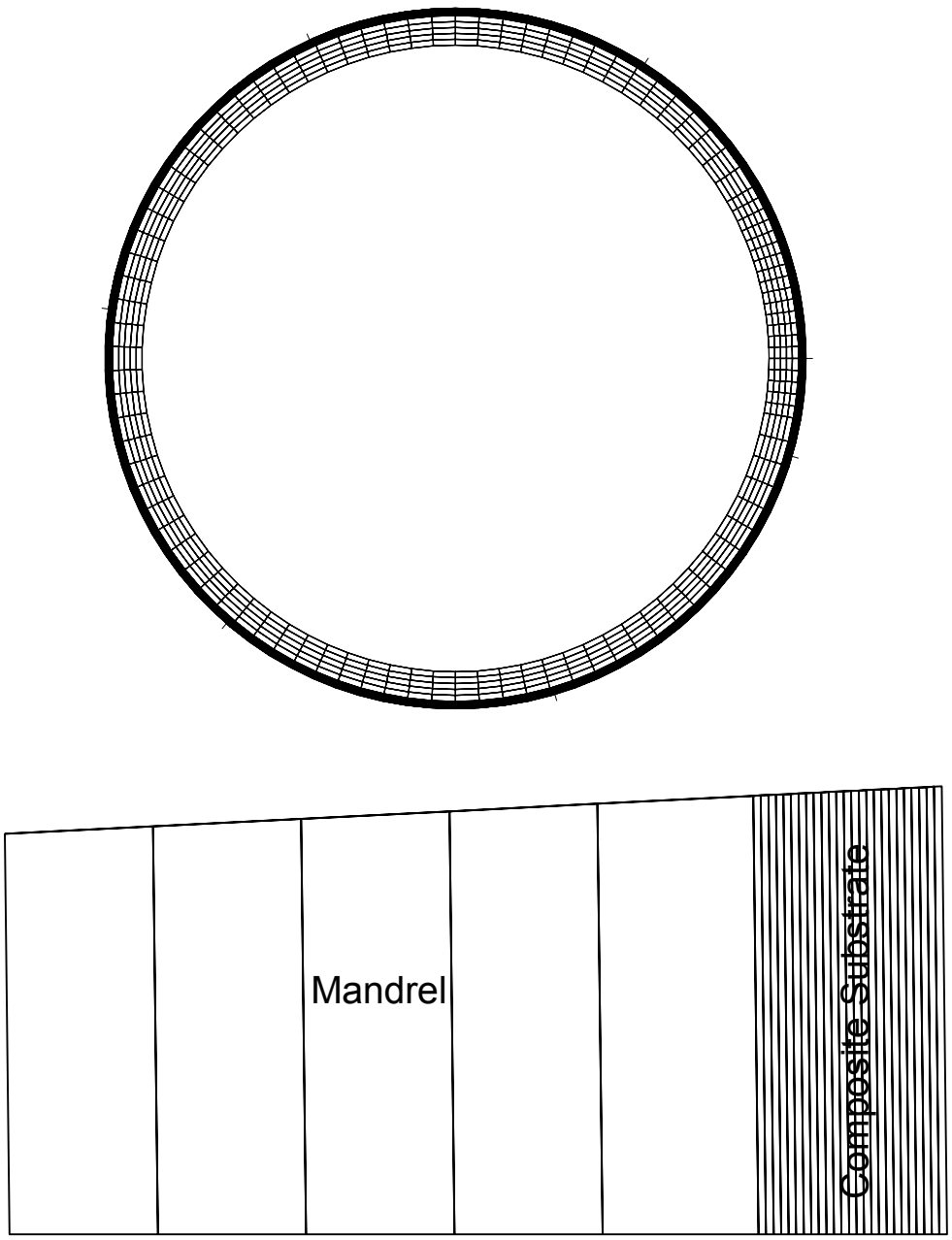

Figure 3.9 Mesh for the heat transfer simulation of substrate cylinder heating

Table 3.1 Input material parameters for heat transfer calculation

Properties	**APC-2**	**Aluminum**
Density (kg/m^3)	1562	2700
Specific Heat $(J/^oK)$	1425	905
Thermal Conductivity Longitudinal (W/m^oK)	6.0	237
Thermal Conductivity Transverse (W/m^oK)	0.72	237

Table 3.2 Input boundary condition parameters for heat transfer analysis

Inner-surface Temperature T_i (^oC)	**Air Film Coefficient** h_a $(W/m^2\ ^oK)$	**Air Temperature** T_a (^oC)	**Hot Gas Film Coefficient** h_{hg} $(W/m^2\ ^oK)$	**Hot Gas Temperature** T_{hg} (^oC) see Figure 3.2		
				T_1	T_2	T_3
65	10	25	280	250	575	500

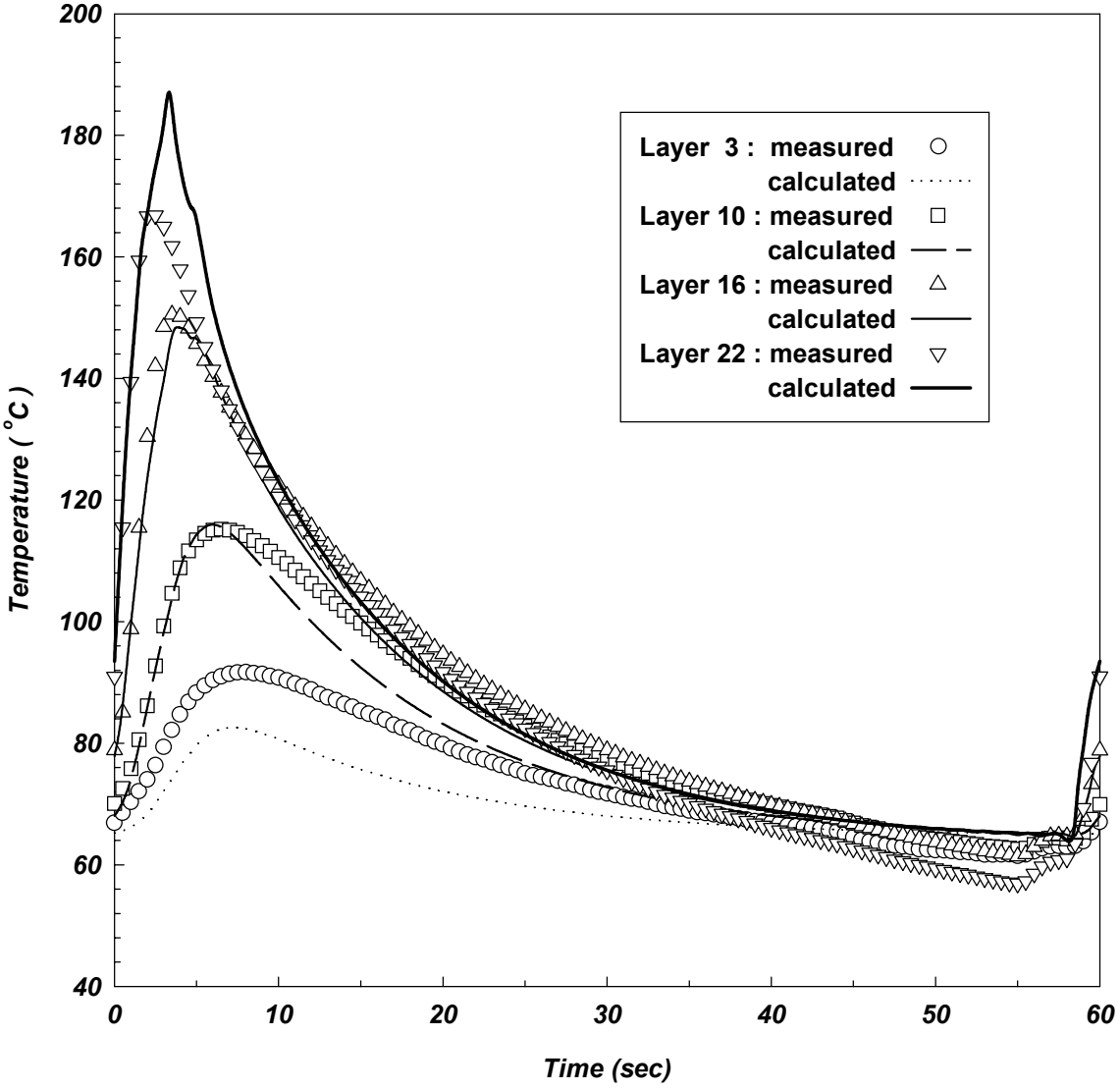

Figure 3.10 Comparisons between the measured and calculated temperatures at a winding speed of 1 rpm

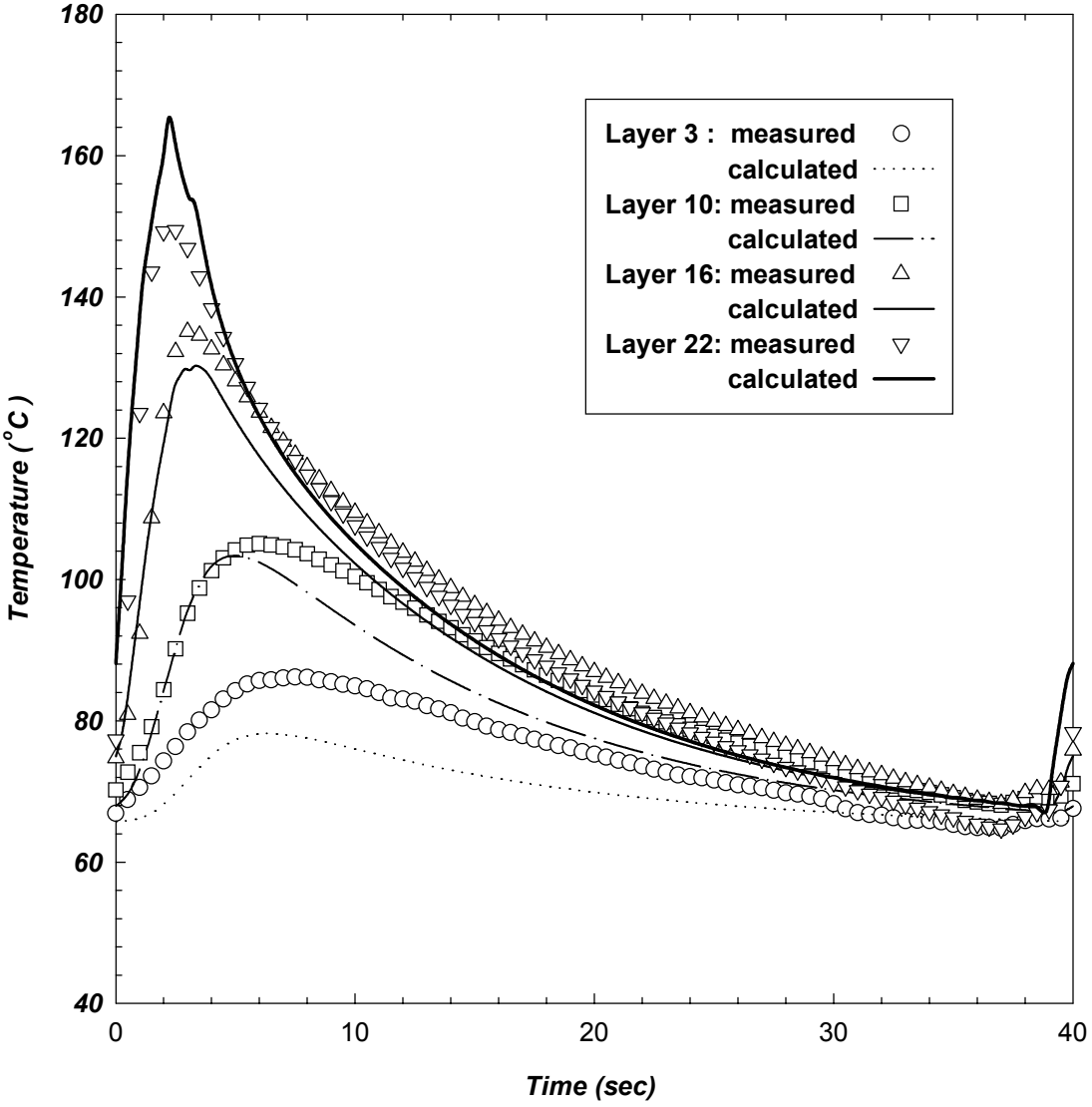

Figure 3.11 Comparisons between the measured and calculated temperatures at a winding speed of 1.5 rpm

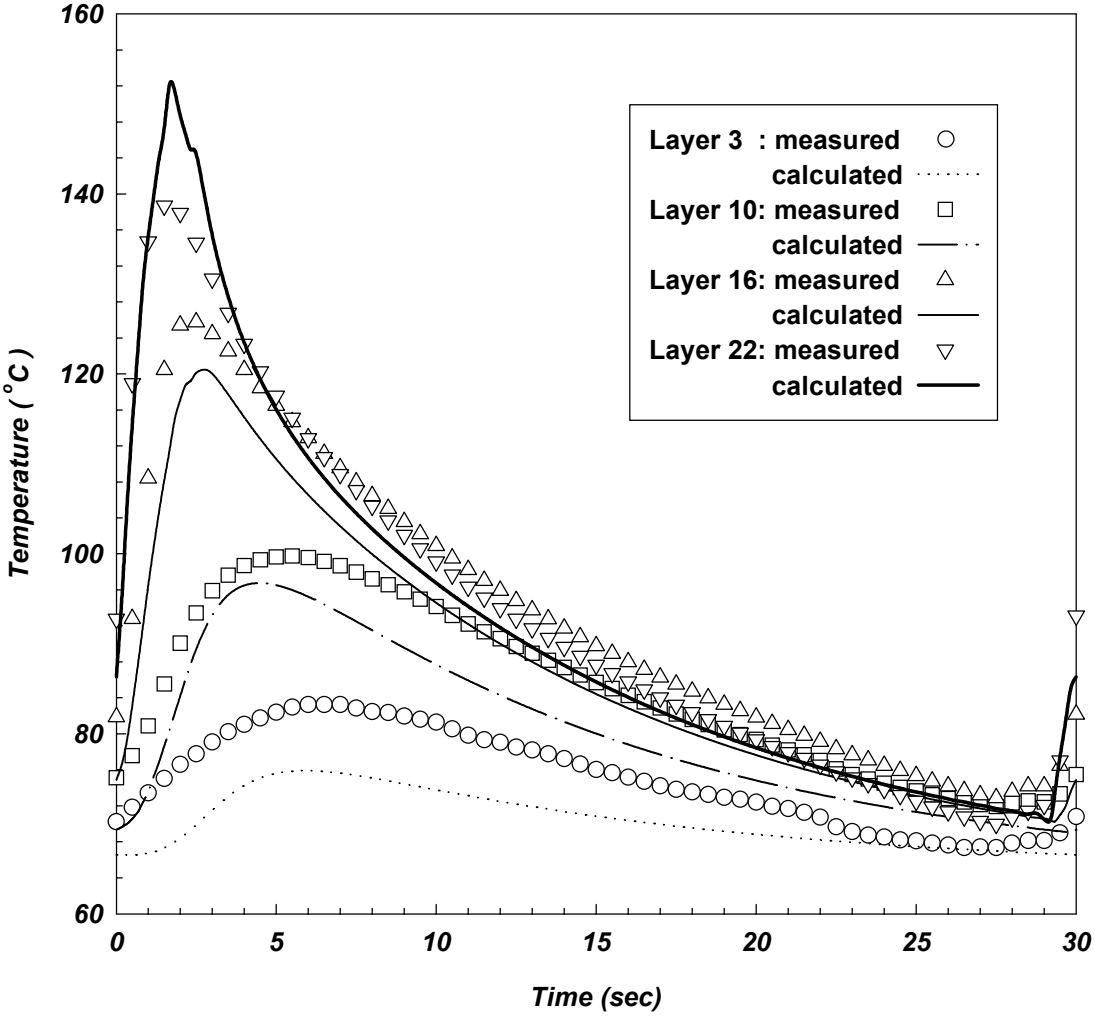

Figure 3.12 Comparisons between the measured and calculated temperatures at a winding speed of 2 rpm

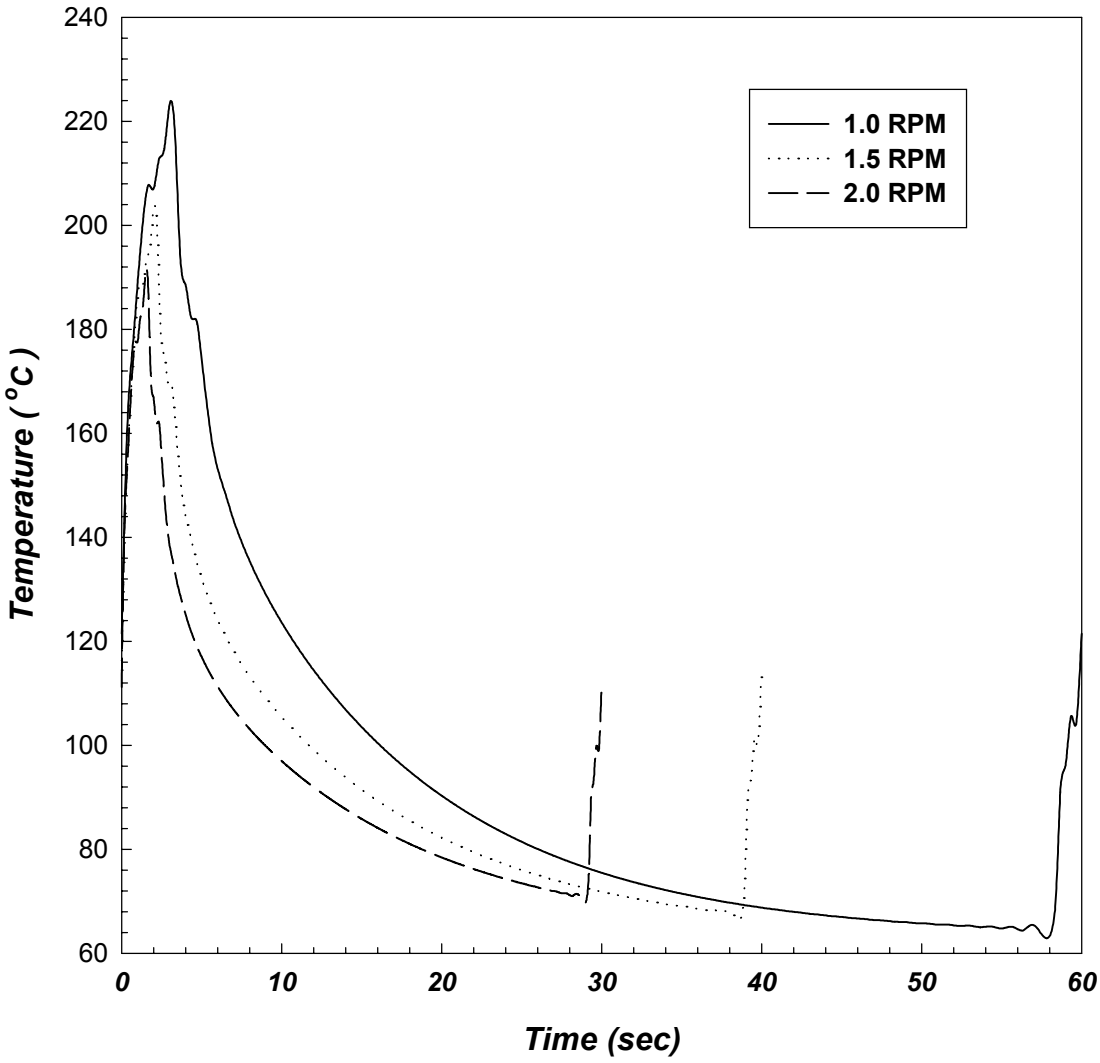

Figure 3.13 The impact of winding speed on the maximum temperature on the outermost surface. The winding speeds are denoted in the inset.

3.3 Simulation on Heating of Towpreg

In the previous section it was concluded that the hot-air heater used in the on-line consolidation system was unable to create a molten zone on the surface of the substrate. A two-dimensional finite element program was constructed to determine the towpreg temperature before entering the nippoint and verify that the hot-air heater could melt the resin of the incoming towpreg.

3.3.1 Governing Equation and Boundary Conditions

During winding, towpreg continuously passes through the heating zone as shown schematically in Figure 3.14. In order to simulate the towpreg motion, the coordinate system is placed at the location of the hot-air heater and moves in the direction opposite to the motion of the towpreg. A quasi-steady state is assumed to prevail through the process. In the Eulerian framework, the problem is formulated as a steady-state conduction heat transfer problem and the governing equation for energy balance becomes,

$$K_{xx}\frac{\partial}{\partial x}\left(\frac{\partial T}{\partial x}\right)+K_{zz}\frac{\partial}{\partial z}\left(\frac{\partial T}{\partial z}\right)=\rho C_p\frac{\partial T}{\partial x}(-v_x) \tag{3.42}$$

where, T is the temperature, K_{xx} and K_{zz} are the composite thermal conductivities in x and z directions, respectively. v_x is the velocity of the moving coordinate system, ρ is the mass density of the towpreg, and C_p is the specific heat. The moving coordinate system velocity v_x is related with the mandrel winding speed ω,

$$v_x=\omega R \tag{3.43}$$

where, R is the radius of the substrate cylinder.

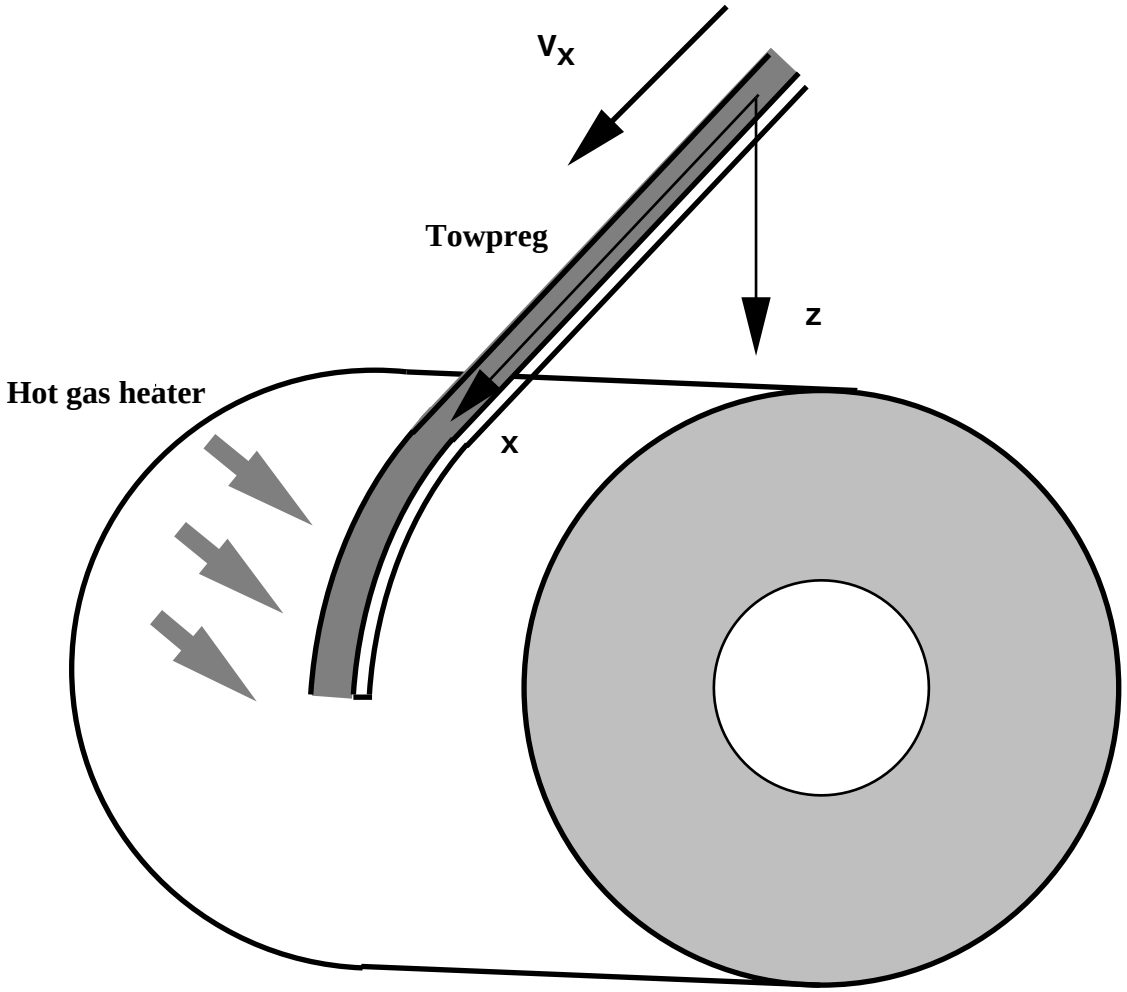

Figure 3.14 Schematic of towpreg heating

Note that,

$$\begin{aligned} K_{xx} &= K_L \\ K_{zz} &= K_T \end{aligned} \tag{3.44}$$

where, K_L and K_T are the longitudinal and transverse conductivities, respectively.

The thermal boundary conditions for the model are illustrated in Figure 3.15. The top surface is heated by the hot air and a forced convection boundary condition is applied. For the bottom surface on the compaction roller, an adiabatic boundary condition is assumed. The left edge is also assumed to be adiabatic. For the region to the right of the heated zone, both the top surface and the bottom surface are subject to free convection. The right edge temperature is prescribed to be air temperature. The boundary conditions of the problem are summarized as follows:

$$\begin{aligned} T &= T_L && on \quad S_1 \\ K_{zz}\frac{\partial T}{\partial z} &= -h_a(T - T_a) && on \quad S_2 \\ -K_{zz}\frac{\partial T}{\partial z} &= -h_a(T - T_a) && on \quad S_6 \\ K_{zz}\frac{\partial T}{\partial z} &= -h_{hg}(T - T_{hg}) && on \quad S_3 \\ K_{xx}\frac{\partial T}{\partial x} &= 0 && on \quad S_4 \\ -K_{zz}\frac{\partial T}{\partial z} &= 0 && on \quad S_5 \end{aligned} \tag{3.45}$$

where, T_L is the prescribed temperature, h_a is the film coefficient, h_{hg} is the hot gas film coefficient, T_a is the air temperature and T_{hg} is the hot gas temperature. Note that the hot gas temperature is not uniform in the heating zone. For simplification, a step function is used to model this variation.

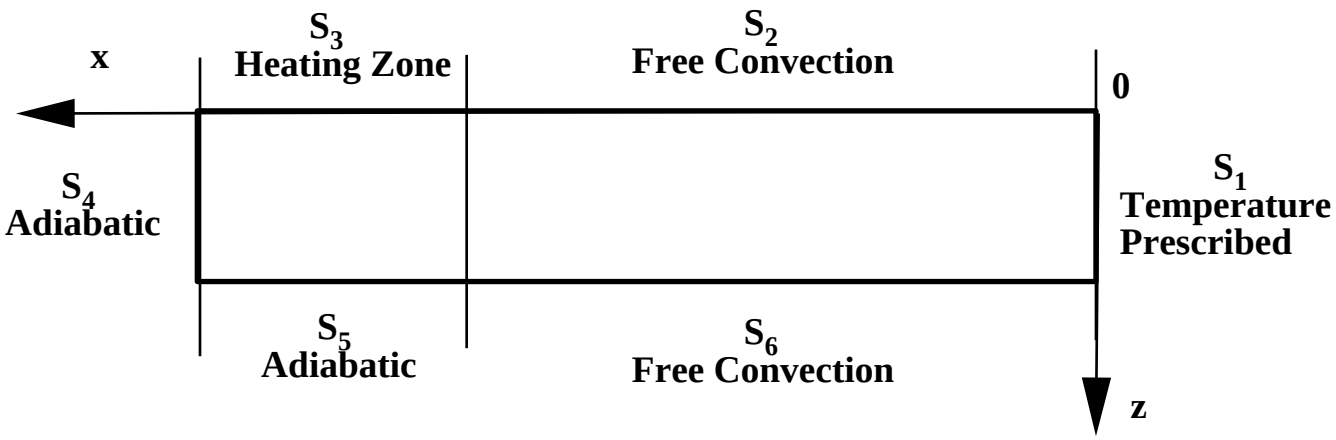

Figure 3.15 Boundary conditions for towpreg heating problem

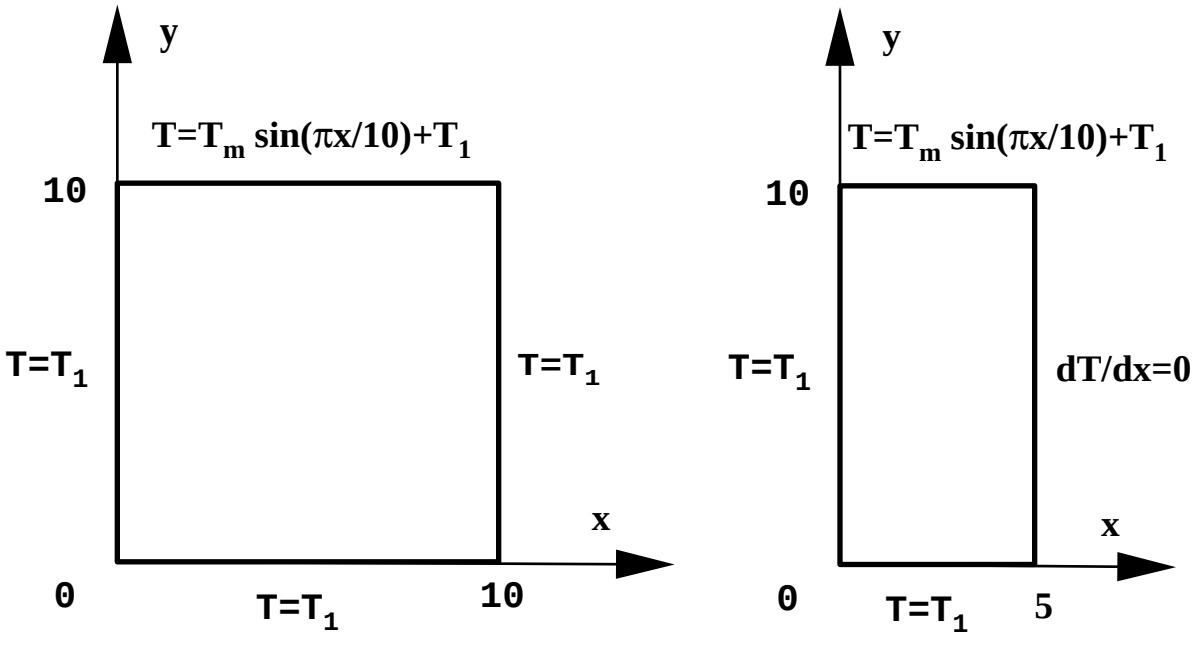

Figure 3.16 Heat transfer problem in a plate with prescribed boundary conditions

3.3.2 Finite Element Formulation and Accuracy Evaluation

Following the standard procedure of Galerkin's method [54], the finite element formulation of the towpreg heat transfer problem can be obtained

$$K_{ij}T_j = P_i \tag{3.46}$$

The matrices K and P are the global stiffness matrix and load vector, respectively and they can be assembled from the element stiffness matrices and load vectors:

$$\begin{aligned} [K_{ij}] &= \sum [K_{mn}]^e \\ [P_i] &= \sum [P_m]^e \end{aligned} \tag{3.47}$$

where

$$\begin{aligned} K_{mn}{}^e &= K_{mn}{}' + K_{mn}{}'' + K_{mn}{}''' \\ P_m{}^e &= \int_{(S_2 \cup S_6)\cap\Omega^e} h_a T_a N_m d\Gamma + \int_{S_3\cap\Omega^e} h_{hg} T_{hg} N_m d\Gamma \\ K_{mn}{}' &= \iint_{\Omega^e} (K_{xx}\frac{\partial N_m}{\partial x}\frac{\partial N_n}{\partial x} + K_{zz}\frac{\partial N_m}{\partial z}\frac{\partial N_n}{\partial z}) d\Omega \\ K_{mn}{}'' &= \iint_{\Omega^e} -\rho C_p v_x N_m \frac{\partial N_n}{\partial x} d\Omega \\ K_{mn}{}''' &= \iint_{(S_2 \cup S_6)\cap\Omega^e} h_a N_m N_n d\Gamma + \iint_{S_3\cap\Omega^e} h_{hg} N_m N_n d\Gamma \end{aligned} \tag{3.48}$$

and, N_m and N_n are shape functions. Four node quadrilateral elements and the corresponding shape functions are used in the study.

The accuracy of the finite element code was verified with a test problem where the analytical solution exists. Consider a two-dimensional square plate (10 cm x 10 cm) as shown in figure 3.16. Temperature is prescribed on the boundaries:

$$\begin{aligned} T &= T_1 && x = 0 \\ T &= T_1 && x = 10\ cm \\ T &= T_1 && y = 0 \\ T &= T_m \sin(\frac{\pi}{10}x) + T_1 && y = 10\ cm \end{aligned} \tag{3.49}$$

In the study, both T_1 and T_m are given as $25^o C$. The temperature at any point (x, y) on the plate is expressed as [55]

$$T = T_m \frac{\sinh(\pi y/10)}{\sinh(\pi)} \sin(\frac{\pi x}{10}) + T_1 \tag{3.50}$$

As shown in Figure 3.17, the exact solution and the finite element solution compare well.

3.3.3 Results

A two dimensional finite element model was developed in the previous sections to study whether the hot-air heater could melt the resin of incoming towpreg. APC-2 towpreg was used in the investigation and the resin's melt temperature is $345^o C$.

The calculated towpreg temperatures before entering the nippoint for different winding speeds (1.0 rpm, 1.5 rpm, and 2.0 rpm) are listed in Table 3.3. As indicated in the Table, the hot–air heater is able to melt the towpreg resin under the specified processing conditions. Mandrel winding speed significantly affects the heating of towpreg, and thus affects bonding behavior. For a specified hot-air heater temperature, high winding speed causes insufficient heating which yields insufficient bonding between the towpreg and composite substrate and a low winding speed may cause overheating and thermal degradation of the towpreg resin. The finite element model of towpreg heating can be used to predict the towpreg temperature and to provide operational limits to avoid insufficient heating or thermal degradation.

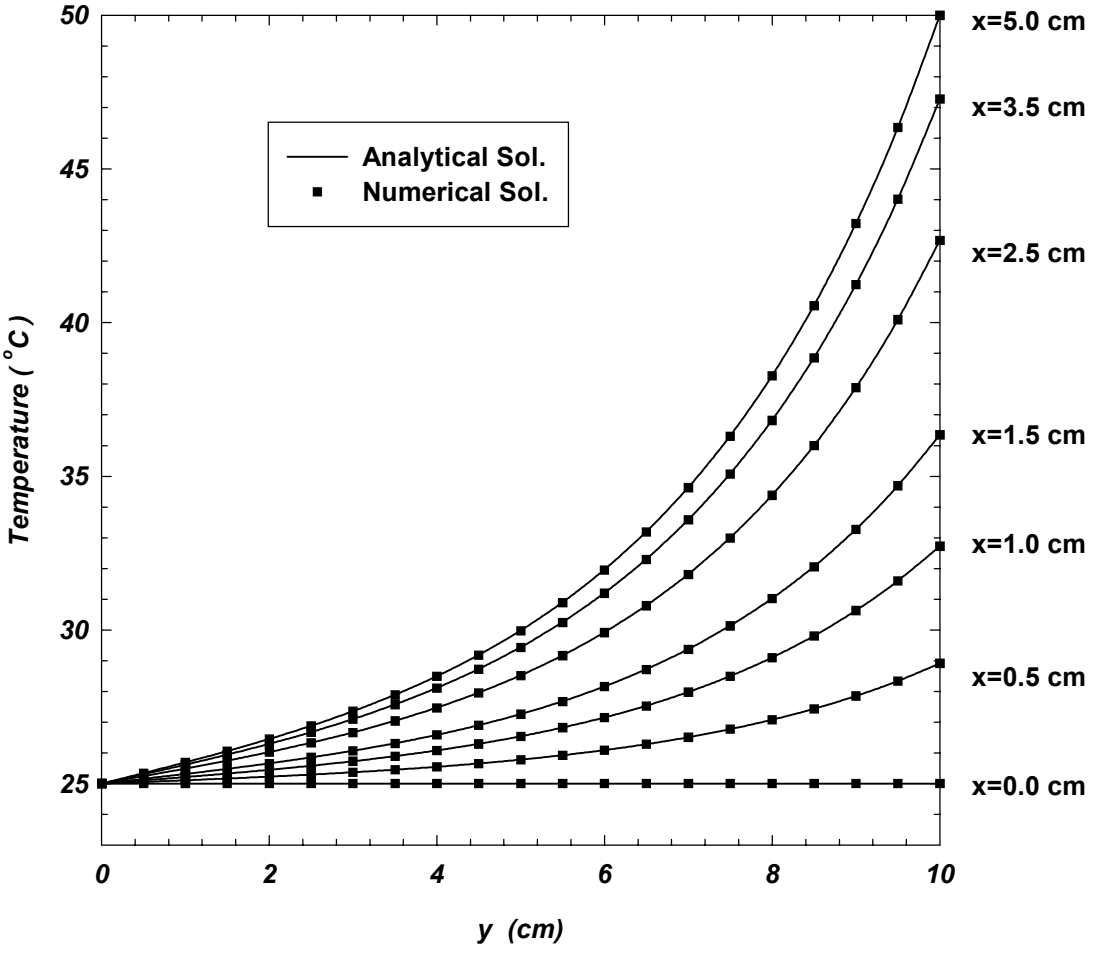

Figure 3.17 Temperature as a function of position (x,y) in the plate. Comparison between the FEM solution and analytical solution. (Eqn 3.50)

Table 3.3 The towpreg temperature before entering the nippoint

Mandrel Winding Speed (rpm)	1.0	1.5	2.0
Temperature (^{o}C)	482	434	365

Chapter 4 Consolidation Submodel

4.1 Introduction

In the on-line consolidation process of thermoplastic composites, heat and pressure are applied to the system to consolidate individual plies into a laminate by bonding at the interfaces. To form good contact and bonding, the major mechanisms, intimate contact and autohesion must occur sequentially or simultaneously.

Incomplete consolidation results in high void content and seriously degrades the interlaminar shear strength of the laminate. Very small shear loads may cause failure of a composite part by delamination. Other phenomenon such as warpage and residual stresses may also occur due to improper consolidation. Therefore, accurate modeling of the on-line consolidation process plays an important role in ensuring the quality of the resulting composite structure. The models to simulate intimate contact and healing are presented in the following sections.

4.2 Intimate Contact Model

In the present study, the intimate contact model developed by Lee and Springer [23] was adopted and used to calculate the progression of the bonding progress during the placement of subsequent layers onto the composite substrate. Since the towpreg surfaces are uneven, spatial gaps exist between the adjacent ply surfaces prior to the application of heat and pressure. The irregular tow surface is represented by a series of uniform rectangular elements of height a, width b, and spacing w. Under pressure and heat, the element height decreases, the element width increases, and the element spacing, which represents the spatial gap, decreases to zero (Figure 4.1). Therefore, the degree of intimate contact is defined as

$$D_{ic} = \frac{b}{w_0 + b_0} \tag{4.1}$$

where b_0 and b are the initial ($t \le 0$) and instantaneous (at time t) widths of each rectangular element respectively, and w_0 is the initial distance between two adjacent elements. When b is equal to the sum of w_0 and b_0, the degree of intimate contact reaches unity and the plies are in complete contact. The deformation and flow of the rectangular elements under pressure and heat can be modeled as a laminar, one-dimensional "squeezing" flow between two parallel plates. Thus the following expression for the degree of intimate contact D_{ic} [23] is derived:

$$D_{ic} = \frac{1}{1+\frac{w_0}{b_0}}\left[1+5\frac{P_{app}}{\eta_0}(1+\frac{w_0}{b_0})(\frac{a_0}{b_0})^2 t\right]^{\frac{1}{5}} \tag{4.2}$$

where P_{app} is the applied pressure, a_0 is the initial height of each rectangular element, and η_0 is the zero-shear-rate viscosity of the resin, which is a function of processing temperature.

For the filament winding process, P_{app} is the pressure applied by the compaction roller to the substrate cylinder (Figure 4.2). Under an applied force f, the roller is in contact with the composite through an arc length $g-h$ (Figure 4.2). The distance between g and h is denoted by l_c. Then P_{app} can be written as

$$P_{app} = \frac{f}{H_r l_c} \tag{4.3}$$

where H_r is the width of the compaction roller. The contact time t is related with the contact length as

$$t = \frac{l_c}{\omega r_c} \tag{4.4}$$

where r_c is the radius of the substrate cylinder.

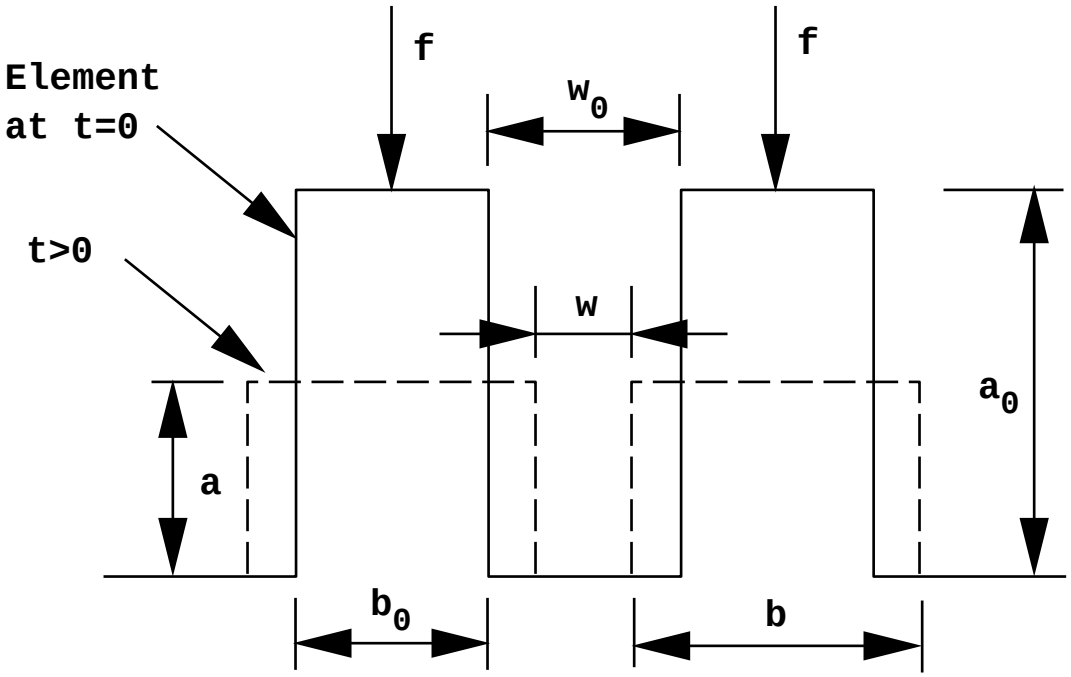

Figure 4.1 Deformation of the elements during the formation of intimate contact

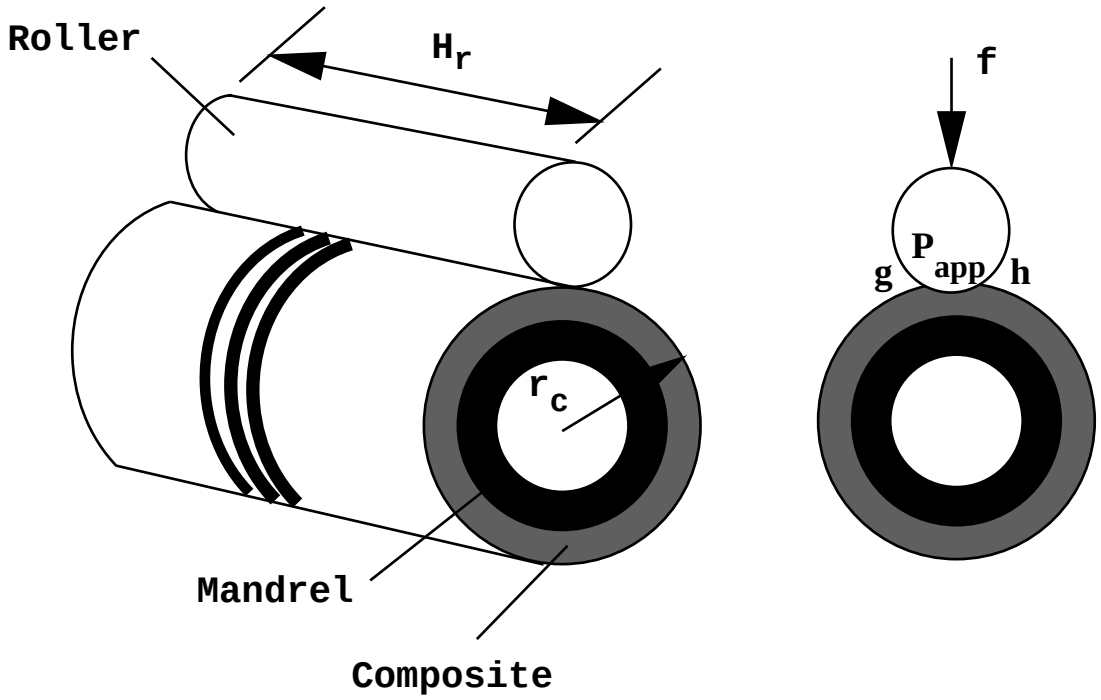

Figure 4.2 Interaction of the roller and the composite in filament winding

Substituting equations (4.3) and (4.4) into equation (4.2), the degree of intimate contact for filament winding process may be calculated by the following expression [12]

$$D_{ic} = \frac{1}{1+\frac{w_0}{b_0}}\left[1+5(1+\frac{w_0}{b_0})(\frac{a_0}{b_0})^2 \frac{f}{\omega r_c H_r}\frac{1}{\eta_0}\right]^{\frac{1}{5}} \tag{4.5}$$

Note that the initial degree of intimate contact D_{ic}^0 $(t \le 0)$ is defined in equation (4.6):

$$D_{ic}^0 = \frac{b_0}{w_0 + b_0} = \frac{1}{1+\frac{w_0}{b_0}} \tag{4.6}$$

Substituting equation (4.6) into equation (4.5) gives the final expression for the degree of intimate contact for the thermoplastic filament winding process:

$$D_{ic} = D_{ic}^0\left[1+5\frac{1}{D_{ic}^0}(\frac{a_0}{b_0})^2 \frac{f}{\omega r_c H_r}\frac{1}{\eta_0}\right]^{\frac{1}{5}} \tag{4.7}$$

D_{ic}^0 is assumed to be 0.5 for the first pass. The degree of intimate contact reached after a pass should be taken as initial degree of intimate contact for the calculation of the subsequent pass.

4.3 Autohesion Model

Once two adjacent interfaces come into contact, the mechanism controlling interply bond formation during processing of thermoplastic composites is recognized to be autohesion [23]. During autohesion, segments of the chain like molecules diffuse across the interface (Figure 4.3). The extent of the molecular diffusion increases with time. After sufficient time has elapsed, some of the chains will have diffused across the interface and entangled with molecular chains on the other side of the interface. Hence, the interface is no longer distinguishable from the bulk polymer.

The motion of a chain in an amorphous polymer has been modeled by the reptation theory [27-29]. The chain is assumed to move in a fixed isothermal network and is considered to be confined in a tube of length L. As the chain moves in the tube, its extremities exit the tube. Then the chain ends, called minor chain, are free to move (Figure 4.4). The length of the minor chain, l, varies with the square root of time as following,

$$\frac{l}{L} = \left(\frac{t}{T_r} \right)^{\frac{1}{2}} \tag{4.8}$$

where T_r, the reptation time, is defined as the time at which the chain has totally exited its original tube $(l = L)$. T_r is a strong function of temperature. Researchers [27-33] have attempted to characterize the extent of autohesion by measuring the interply bond strength and calculating the degree of autohesion, D_{au}. It is defined as,

$$D_{au} = \frac{S}{S_\infty} \tag{4.9}$$

where S is the bond strength at time t and S_∞ is the ultimate bond strength, i.e., the strength of a completely bonded interface. And the time dependence of the interfacial bonding strength was found to be

$$\frac{S}{S_\infty} = \left(\frac{t}{T_r} \right)^{\frac{1}{4}} \tag{4.10}$$

For the nonisothermal processes, the temperature history is divided into infinitesimal time intervals during which the temperature is assumed constant. In each isothermal step, the healing theory can be applied [30]. Following this approach by Bastien and Gillespie [30], Sonmez and Hahn developed their nonisothermal autohesion model [26]. The model of Sonmez and Hahn was employed in the present study.

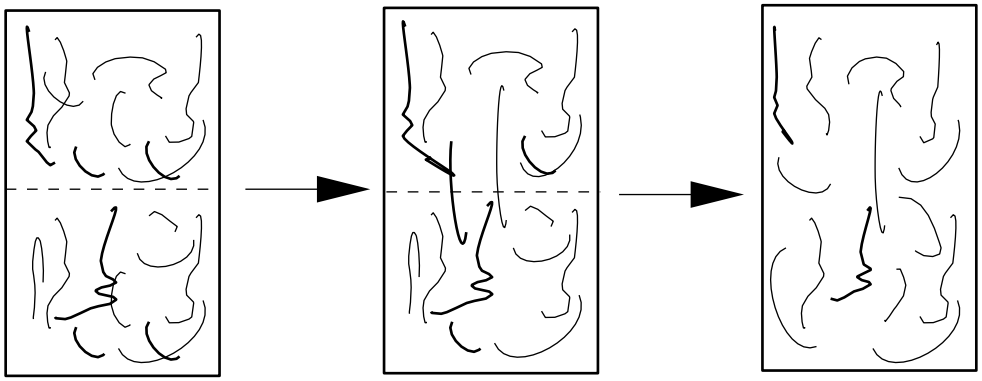

TIME	**t=0**	**t>0**	**t_{oo}**
STRENGTH	**S=0**	**S**	**S_{oo}**
AUTOHESION	**$D_{au}=0$**	**$D_{au}=S/S_{oo}$**	**$D_{au}=1$**

Figure 4.3 Illustration of the autohesion process

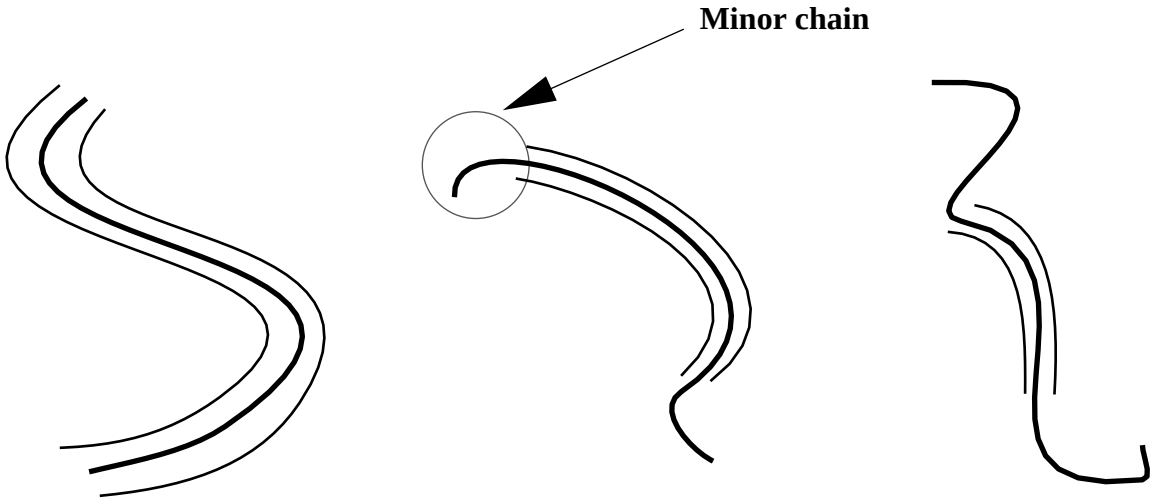

Figure 4.4 Minor chain

By differentiating Equation (4.8), Equation (4.11) is obtained as

$$\frac{dl}{L} = \frac{dt}{2\sqrt{tT_r}} \tag{4.11}$$

Integrating Equation (4.11)

$$\int_0^l \frac{ds}{L} = \int_0^t \frac{d\eta}{2\sqrt{\eta T_r}} \tag{4.12}$$

yields

$$\frac{l}{L} = \int_0^t \frac{d\eta}{2\sqrt{\eta T_r}} \tag{4.13}$$

therefore

$$D_{au}(t) = \frac{S}{S_\infty} = \left(\frac{l}{L}\right)^{\frac{1}{2}} = \left(\int_0^t \frac{d\eta}{2\sqrt{\eta\, T_r(\eta)}}\right)^{\frac{1}{2}} \tag{4.14}$$

The relation (4.14) also holds for PEEK films and prepregs [26].

4.4 Bonding Model

During processing, autohesive bonding of the ply interfaces occurs at the areas in intimate contact once the temperature exceeds the glass transition temperature for amorphous polymers or the melt temperature for semicrystalline polymers. Hence, the degree of bonding, D_b is a convolution integral of the degree of intimate contact and the degree of autohesion:

$$D_b(t) = \int_0^t D_{au}(t-\tau)\frac{\partial D_{ic}}{\partial \tau} d\tau \tag{4.15}$$

For the case where autohesion proceeds much faster than intimate contact, the equation is simplified to the expression [26]:

$$D_b \approx D_{ic} \cdot D_{au} \tag{4.16}$$

4.5 Results

Shih and Loos [22] experimentally studied the impact of processing parameters on the bonding quality of filament-wound thermoplastic composites. Nine composite rings, 26-ply thick and 19mm wide, were fabricated with APC-2 towpreg from Fiberite, Inc. Interlaminar shear strength (ILSS) tests were conducted to measure the interlayer bonding quality of each composite ring. The degree of bonding on the test interface is assumed to be proportional to its interlaminar shear strength, i.e.,

$$D_b = \frac{S_{ILSS}}{S_\infty} \tag{4.17}$$

where S_{ILSS} is the strength resulting from the interlaminar shear strength tests and S_∞ is the ultimate bonding strength. For APC-2 composite, an interlaminar shear strength of 71.8MPa was used as S_∞. This is the value of the ILSS for an APC-2 composite fabricated using the manufacturer's recommended processing conditions of $380^o C$ for 5 minutes under a hot press loading at 1380kPa.

In the present study, the bonding model developed in the Section 4.4 is used to calculate the degree of bonding for nine carbon fiber, PEEK matrix APC-2 composite rings that were consolidated under different processing conditions. The additional bonding during the placement of subsequent layers was also investigated in the study. During the placement of subsequent layers, the same interface may experience high temperature and pressure again and the bonding process is resumed. However, as the layers are laid down, the temperature at that interface will gradually decrease. Note that bonding below $270^o C$ was reported to be very slow for PEEK [26]. Accordingly, if the maximum temperature at the interface falls below $270^o C$, bonding calculations are stopped. Figure 4.5 shows the solution procedure used for the bonding analysis.

Input parameters for the bonding analysis are given in Table 4.1. Table 4.2 lists the processing conditions for each ring taken from the experimental study reported by Shih and Loos[22].

Shown in Table 4.3 is the model prediction of bond strength development on different layer interfaces for an APC-2 composite ring consolidated using the processing

conditions for cylinder #2. The bond strength in the cylinder is not uniform in radial direction. The interply bond strengths for the inner layers, closest to the mandrel, are lower than for the intermediate layers in the composite. For the inner layers, the influence of heat loss due to the high thermal conductivity of the aluminum mandrel yields lower nippoint temperature, and hence affects the consolidation process. The degree of bonding for the interface between layer 25 and layer 26, the outermost layer, is low possibly due to heat losses to the ambient. The bond strength continues to increase during the placement of subsequent layers when the maximum temperature on the interface is above $270^{o}C$. For example, the degree of bonding at the interface between layers 20 and 21 is 0.85 after the 21st lay-up and it increases to unity after winding the 22nd layer. Lowest values of the degree of bonding, representing the weakest part for the composite rings, were used to predict the bond strength developed for the composite and compared with the experimental results. Figure 4.6 shows that the model prediction and the experimental results fit well. It can be concluded that for a specified winding speed, a higher nozzle temperature yields higher bond strength; and a slower winding speed results in better consolidation quality for specified nozzle temperature.

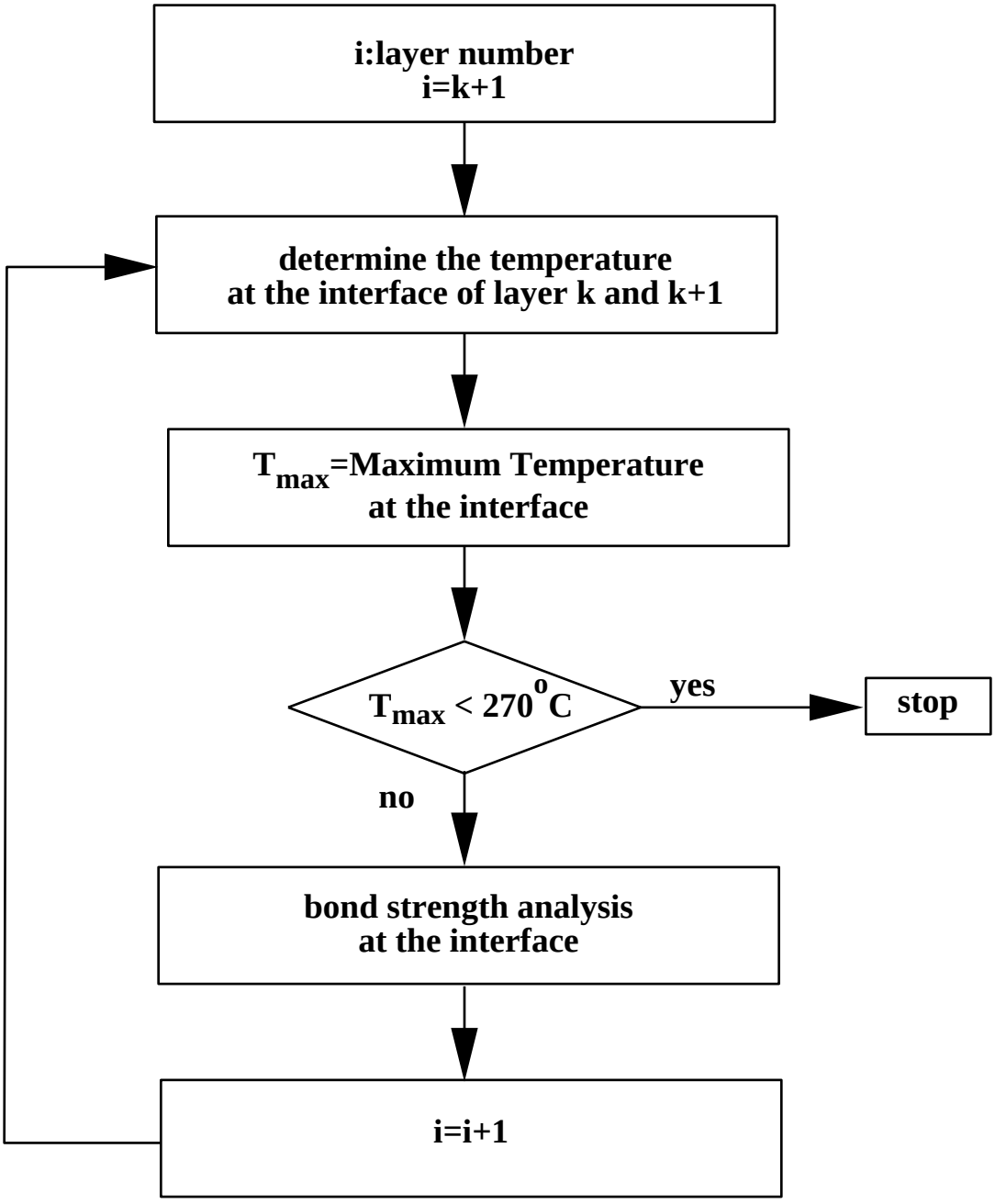

Figure 4.5 The solution procedure for the bonding analysis

Table 4.1 Input parameters for the bonding Analysis

Intimate Contact Model	
Applied force f	55 lb
Width of the compaction roller H_r	2 inch
Geometric ratio a_0 / b_0, Ref. [25]	0.008
Viscosity η_0, Ref. [25]	$\eta_0 = 0.1\exp(4.0617 + \frac{2869}{T(^oK)})$ $Pa \cdot s$
Autohesion Model, Ref. [26]	
The reptation time T_r	$T_r = t_r \exp\left[\frac{E_a}{R}(\frac{1}{T} - \frac{1}{T_{ref}})\right]$
Constant t_r	0.11 sec
Activation energy E_a	57300 J/mol
Universal gas constant R	8.314 J/(K mol)
Reference temperature T_{ref}	673^oK

Table 4.2 Processing Conditions for the nine cylinders

Cylinder Number	**Nozzle Temperature** (^oC)	**Winding Speed (rpm)**
1	635	0.79
2	677	0.46
3	635	1.25
4	635	0.44
5	539	0.46
6	649	0.79
7	576	0.79
8	539	0.99
9	677	0.99

Table 4.3 Bond strength development on different interfaces (Cylinder #2)

Interface	**Lay-up**	D_b	D_{ic}	D_{au}
Layer 1/Layer 2	2nd	0.79	0.79	1.00
Layer 5/Layer 6	6th	0.82	0.82	1.00
Layer10/Layer 11	11th	0.85	0.85	1.00
Layer12/Layer 13	13th	0.85	0.85	1.00
	14th	1.00	1.00	1.00
Layer 20/Layer 21	21st	0.85	0.85	1.00
	22nd	1.00	1.00	1.00
Layer 24/Layer 25	25th	0.85	0.85	1.00
	26th	1.00	1.00	1.00
Layer 25/Layer 26	26th	0.85	0.85	1.00

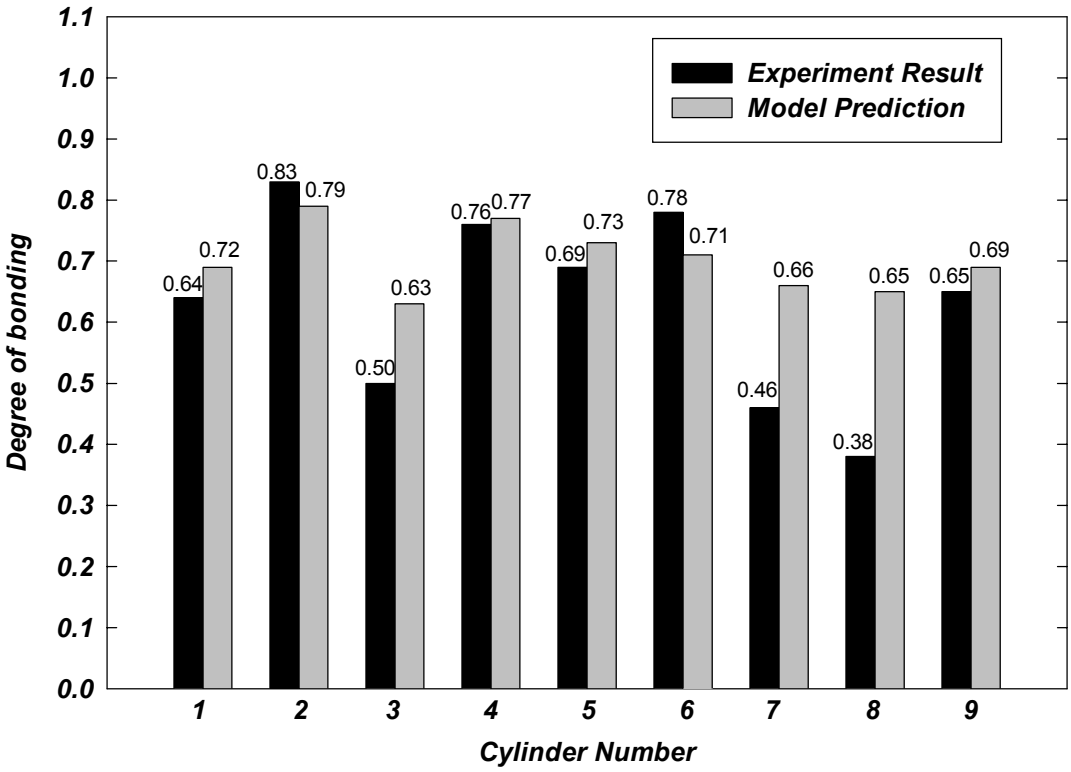

Figure 4.6 Comparison of model prediction and experiment result for the bond strength

Chapter 5 Crystallinity Submodel

For semicrystalline thermoplastic matrix composites, the degree of crystallinity affects significantly the mechanical properties of the composite. Therefore, it is essential to estimate the change in morphology during the process and determine the effects of processing parameters on the crystallization behavior of the matrix in order to control part quality.

Crystallization behavior of thermoplastic matrix composites is a temperature history dependent procedure. In the filament winding process, the temperature history that the material experiences is very complex. The area exposed to the heat source is rapidly heated to the melt and then cooled as the consolidated tow moves away from the nippoint. Hence, initial crystallinity is established. As the winding process continues, the crystallinity may keep changing until the maximum temperature in the existing consolidated layers is below the glass transition temperature. When the polymer is raised to a temperature above its melting temperature, but not high enough to melt the last traces of the crystalline phase, the surviving crystals will serve as nucleation sites on subsequent cooling. Consequently, crystallization and nucleation rates are enhanced. On the other hand, too high a temperature reduces the number of residual nuclei and therefore retards crystallization [8].

The objective of this study is to study the crystallization behavior of the thermoplastic composites during the melting, cooling, remelting, resolidification, and annealing in the filament winding process.

5.1 Crystallization Kinetics Model

In the present study, the model of Sonmez and Hahn [8] for nonisothermal crystallization of APC-2 is adopted. The model involves both crystallization and melting processes to study the crystal growth and the crystallinity development. But in their model, the volume fraction crystallinity at infinite time $Cv(\infty)$ is assumed to be only dependent upon temperature. Actually, cooling rate has a more significant influence on the value of $Cv(\infty)$ during the cooling process while temperature is the dominant factor

to determine $Cv(\infty)$ for the annealing procedure. In the current study, we modified Sonmez and Hahn's model by using different models to calculate $Cv(\infty)$ for the cooling and annealing mechanisms.

Based on the Tobin equation [43-45], the crystallization procedure is described by the following expression:

$$\frac{\alpha(t)}{1-\alpha(t)} = KNt^n + KI^* \int_0^t (t-w)^n [1-\alpha(w)]dw \tag{5.1}$$

where, the first term on the right hand side of the equation represents the heterogeneous nucleation mechanism and the second term the homogeneous nucleation mechanism. w is a dummy integration constant, $\alpha(t)$ is the volumetric relative crystallinity, K contains nucleation and growth parameters, n is an integer whose value depends on the nucleation mechanism and on the form of crystal growth, N is the initial number of heterogeneous nuclei, and I^* is the rate of homogeneous nucleation. It was found experimentally that crystal growth occurs via the formation of three dimensional spherulites and n is equal to 3. The nucleation and growth parameter is described by

$$K = \frac{4}{3}\pi v^3 \tag{5.2}$$

where, v is the radial growth rate of the spherulite. v has the form:

$$v = v_0 \exp(-\frac{E_d}{RT}) \exp(-\frac{\psi_1 T_m^0}{T(T_m^0 - T)}) \tag{5.3}$$

where, v_0 is a universal constant for a semicrystalline polymer ($v_0 \approx 7.5\times10^8 (\mu m/s)$, T_m^0 is an equilibrium melting temperature, E_d is the activation energy of diffusion of crystallizing segments across the phase boundary, and ψ_1 is a constant related to the free energy of formation of a critical nucleus.

The following expression for I^* is used:

$$I^* = I_0 \exp(-\frac{E_d}{RT}) \exp(-\frac{\psi_2 T_m^0}{T(T_m^0 - T)}) \tag{5.4}$$

where ψ_2 is a constant related to the free energy of formation of a growth embryo.

Equation (5.1) describes only isothermal crystallization and an equation to analyze the nonisothermal process is obtained by differentiating equation (5.1):

$$\dot{\alpha}(t) = K_1 \exp(-\frac{3E_d}{RT}) \exp(-\frac{3\psi_1 T_m^0}{T(T_m^0 - T)}) t^2 [1-\alpha(t)]^2 + K_2 \exp(-\frac{4E_d}{RT}) \exp(-\frac{(3\psi_1 + \psi_2)T_m^0}{T(T_m^0 - T)}) \cdot [1-\alpha(t)]^2 \int_0^t (t-w)^2 [1-\alpha(w)] dw \quad (5.5)$$

where,

$$K_1 = 4\pi N v_0^{\ 3} \quad and \quad K_2 = 4\pi I_0 v_0^{\ 3} \quad (5.6)$$

The volume fraction crystallinity $C_v(t)$ is defined as

$$C_v(t) = \alpha C_v(\infty) \quad (5.7)$$

where $C_v(\infty)$ is the volume fraction crystallinity at infinite time. Values for $C_v(\infty)$ during the heating process are determined from data reported by Blundell and Gaskin [56]. Blundell and Gaskin used WAXS to measure the crystallinity of APC-2 that has been quenched into the amorphous state and then post annealed for 30 minutes at different temperatures. During the cooling process, Ozawa's model [48] is adopted to estimate $C_v(\infty)$ for APC-2:

$$C_v(\infty) = -0.03 \ln(\frac{dT}{dt}) + 0.42 \quad (5.8)$$

The crystal melting kinetics is described by

$$C_v(t) = C_v(t_{in})(1 - 0.5 \int_{t_{in}}^{t} \overline{K} dt)^2 \quad (5.9)$$

where t_{in} is the initial time and $\overline{K}$ is described by an Arrhenius relation:

$$\overline{K} = \overline{K}_0 \exp(-\frac{E_a}{RT}) \quad (5.10)$$

Equations (5.5) and (5.7) are used during cooling from the melting temperature T_m to the glass transition Temperature T_g and during heating from glass transition up to $320^o C$. Equation (5.9) is used during heating from $320^o C$ and whenever the temperature is above the melting temperature $(345^o C)$. Below the glass transition temperature, the crystallization rate is assumed to be zero. During heating, the transition temperature between crystallization and melting is chosen to be $320^o C$ because both models predict very small rates at this temperature [8].

The solution procedure used for the crystallinity calculation is shown in Figure 5.1. Table 5.1 presents the input parameters for the model.

5.2 Results

The crystallinity development during winding of nine 26-ply thick, 19 mm wide APC-2 composite rings with different torch temperatures and winding speeds was calculated using the model described in Section 5.1. The crystallinity at the top surface of the 20th ply for the nine cylinders is compared in Table 5.2. It can be concluded that for a specified winding speed, higher torch temperature yields higher crystallinity, and lower winding speed results in higher crystallinity for a specified torch temperature. Figure 5.2 shows the temperature profiles and the corresponding crystallinity development at the top surface of the 20th ply as the 21st layer and the subsequent layers are being wound. It is shown that crystallization continues for subsequent windings until the maximum temperature in the layer falls below the glass transition temperature.

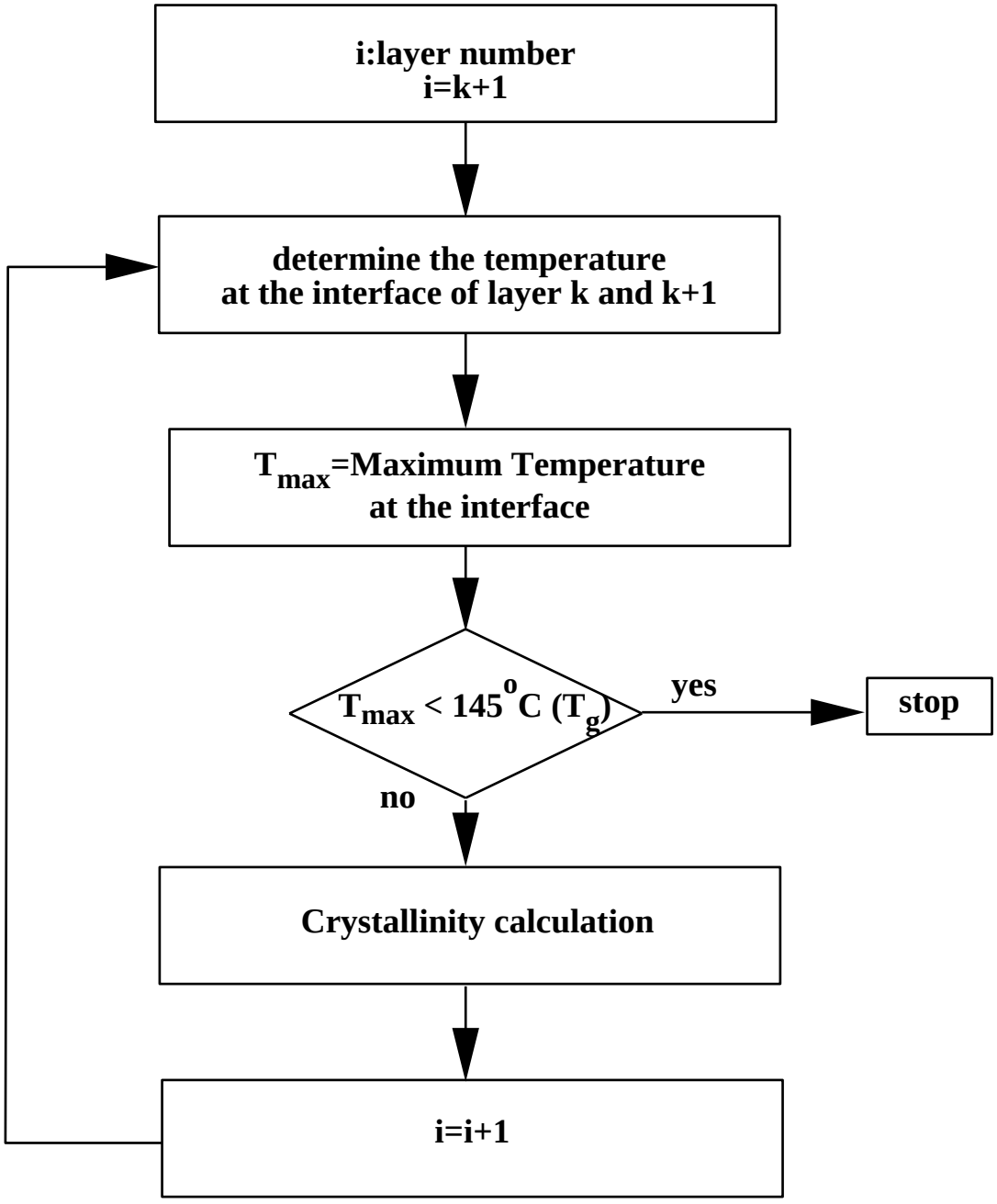

Figure 5.1 The solution procedure for the crystallinity development analysis

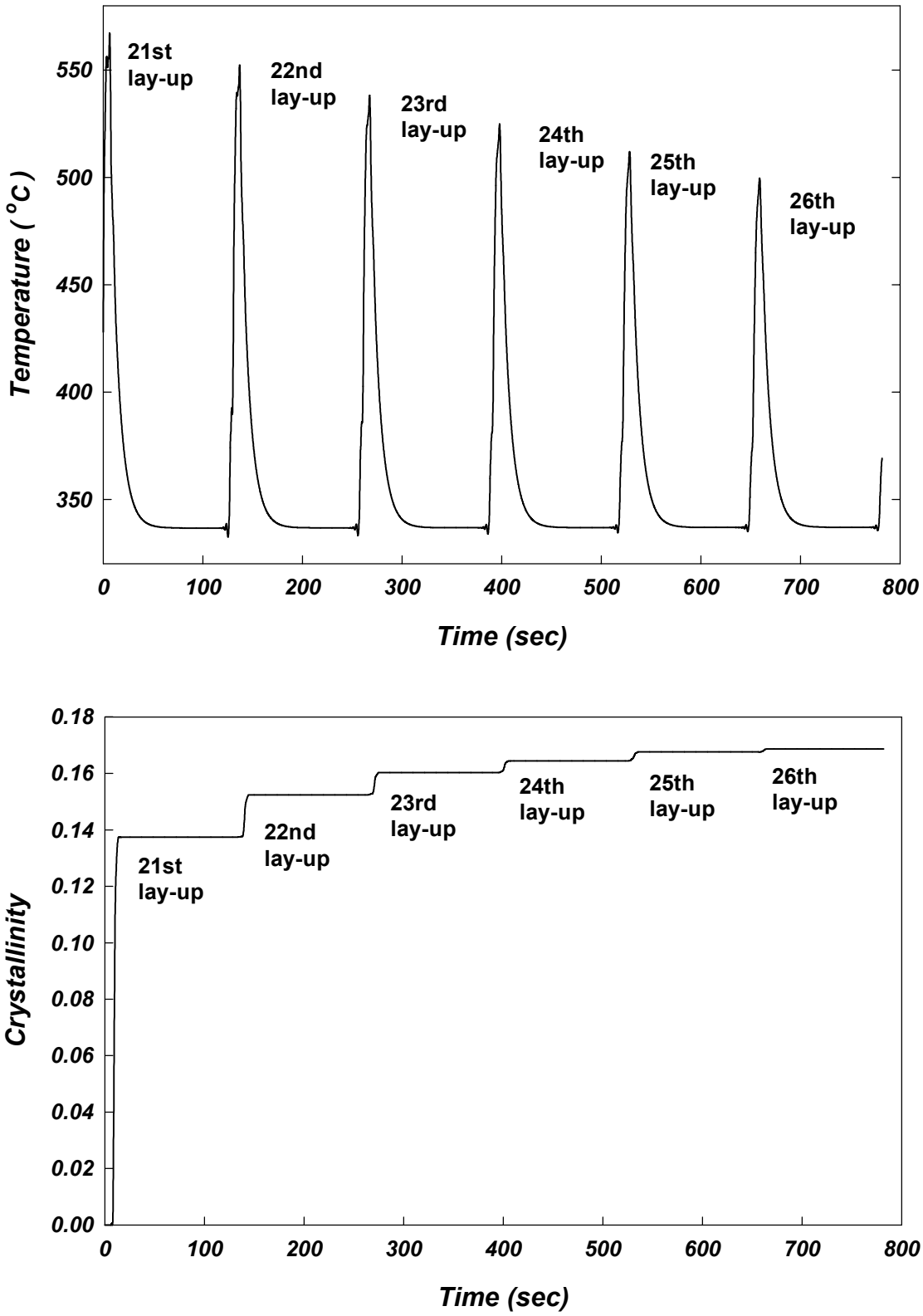

Figure 5.2 Temperature profiles experienced by the top surface of the 20th ply during winding and the corresponding crystallinity development

Table 5.1 Input parameters for the crystallinity calculation

Crystallization model Equation (5.5)	
K_1, kinetic constant [53]	$9.03\times10^{24}\ s^{-3}$
K_2, kinetic constant [53]	$9.32\times10^{38}\ s^{-4}$
ψ_1 kinetic constant [53]	$8.02\times10^{2}\ K$
ψ_2 kinetic constant [53]	$1.79\times10^{3}\ K$
E_d, activation energy for diffusion [53]	$1.52\times10^{4}\ cal/mol$
T_m^0, equilibrium melting temperature [53]	$385C$
R, universal gas constant	$8.314 J/mol\cdot K$
Melting model Equation (5.10)	
$\overline{K}_0$, kinetic constant [56]	$\exp(73)\ s^{-1}$
E_a, activation energy for melting [56]	$397 KJ/mol$

Table 5.2 Crystallinity development comparison in different manufacturing conditions

Cylinder Number	**Nozzle TEMPERATURE** (^oC)	**Winding Speed (rpm)**	**Crystallinity**
1	635	0.79	0.104
2	677	0.46	0.168
3	635	1.25	0.082
4	635	0.44	0.134
5	539	0.46	0.153
6	649	0.79	0.105
7	576	0.79	0.096
8	539	0.99	0.083
9	677	0.99	0.089

Chapter 6 The Effect of Preheating

In this chapter, the heat transfer analysis, the consolidation model, and the crystallization model are integrated to study the temperature profiles, consolidation development and crystallization behavior in the manufacture of a 30-ply APC-2 composite ring. Especially, the effect of preheat temperature was investigated. In the simulation, the towpreg was continuously wound onto an aluminum mandrel. The inner radius of the mandrel was 0.1m and the outer radius 0.125m. The hot air heater temperature was $677\,^{o}C$ and the mandrel winding speed was 0.46 rpm. Three different substrate preheat temperatures $65\,^{o}C$, $80\,^{o}C$, and $100\,^{o}C$ are investigated. Figures 6.1, 6.2, and 6.3 show the temperature profiles and Figures 6.4, 6.5, 6.6 illustrate the crystallinity development on the top surface of layer 20 for substrate preheat temperatures $65\,^{o}C$, $80\,^{o}C$, and $100\,^{o}C$, respectively. The towpreg temperature before enter the nippoint was calculated to be $633\,^{o}C$ and the preheat temperature of the substrate does not affect the calculation. Table 6.1 shows the variation of the degree of bonding and crystallinity with the preheat temperature of the substrate. It lists the lowest values of the degree of bonding for the composite cylinder, which occur at the interface between the first plies and the second plies, and the crystallinity on the top surface of layer 20. It can be concluded that the higher preheat temperature yields better consolidation and higher crystallinity, therefore, improves the quality of the composite.

Table 6.1 The effect of preheating

Preheat temperature	$65\,^{o}C$	$80\,^{o}C$	$100\,^{o}C$
Lowest value of degree of bonding	0.76	0.77	0.79
Crystallinity on the top surface of layer 20	0.170	0.179	0.195

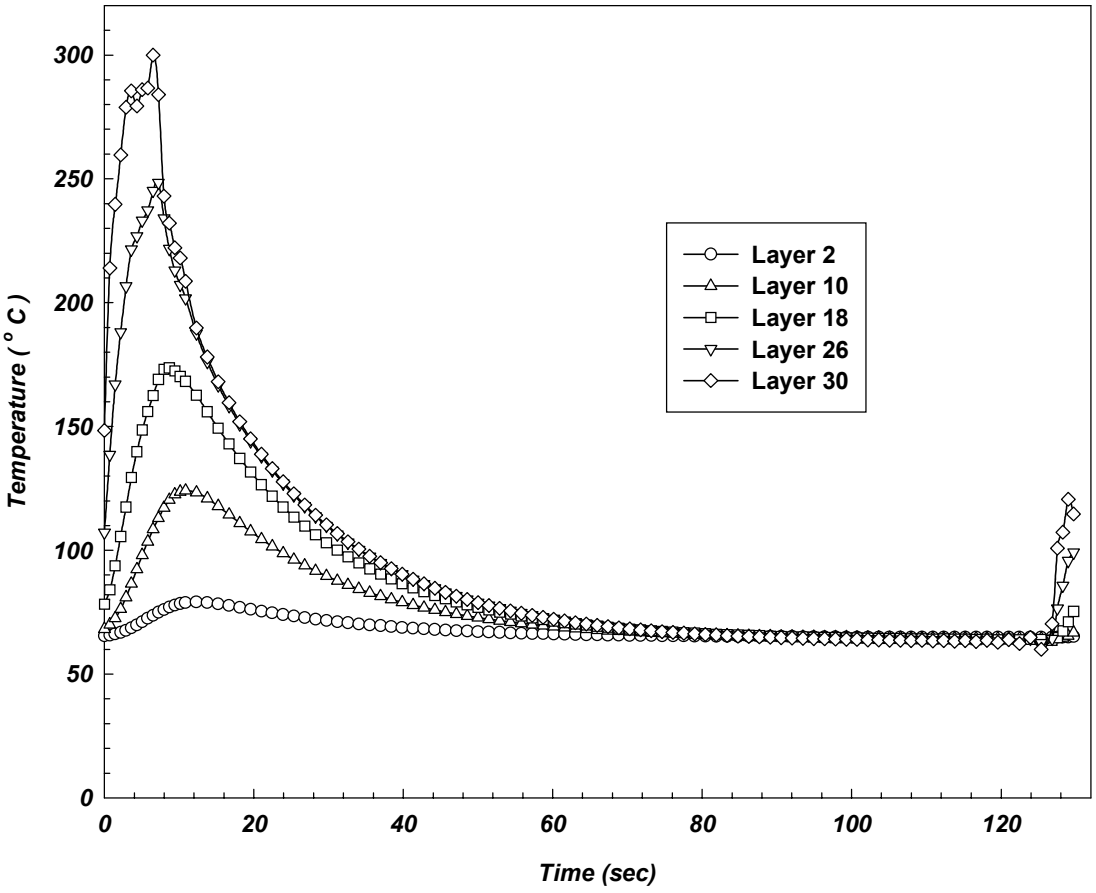

Figure 6.1 Temperature profile of the composite for the substrate preheat temperature of 65 ^{o} C

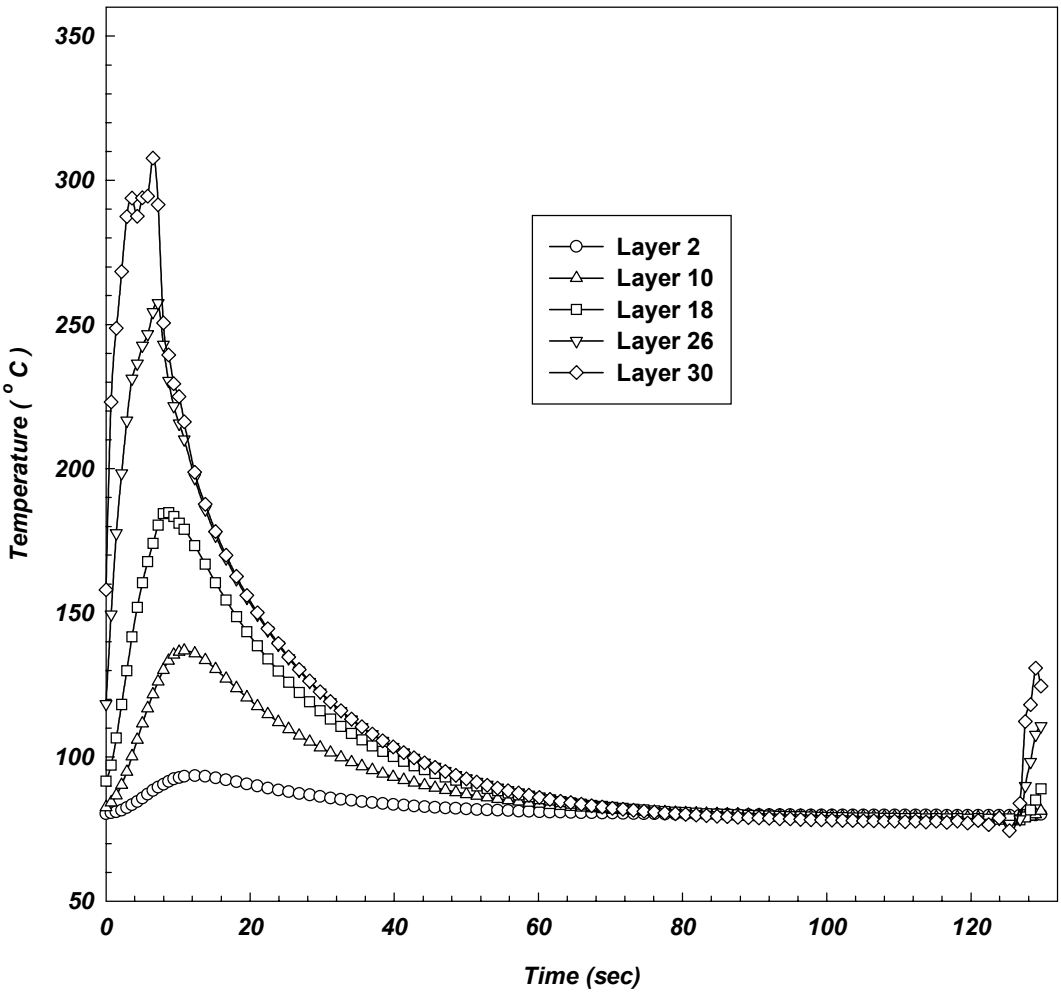

Figure 6.2 Temperature profile in the composite for the substrate preheat temperature of 80 ^{o} C

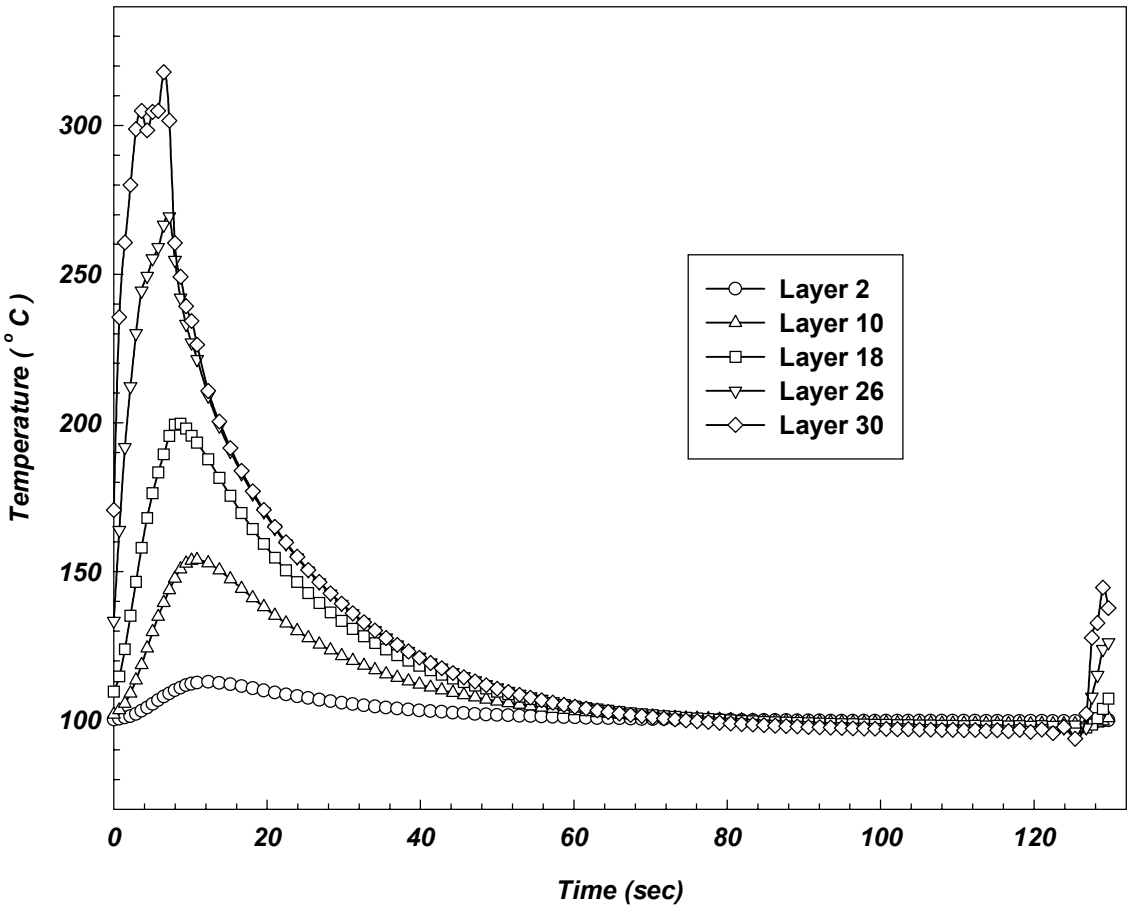

Figure 6.3 Temperature profiles in the composite for the substrate preheat temperature of 100 ^{o}C

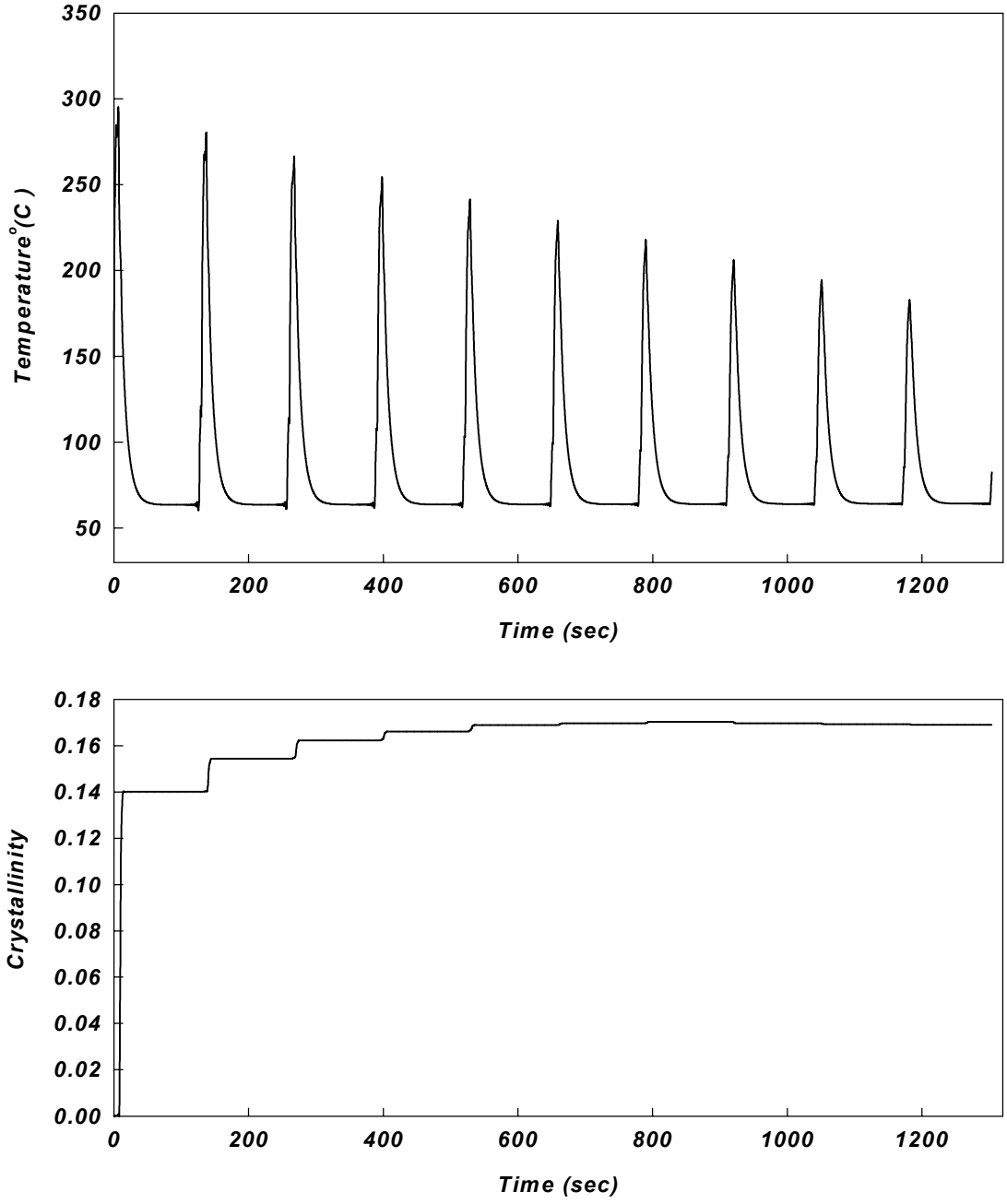

Figure 6.4 Temperature profiles for the top surface of the 20th ply during winding and the corresponding crystallinity development for the preheat temperature of 65 °C

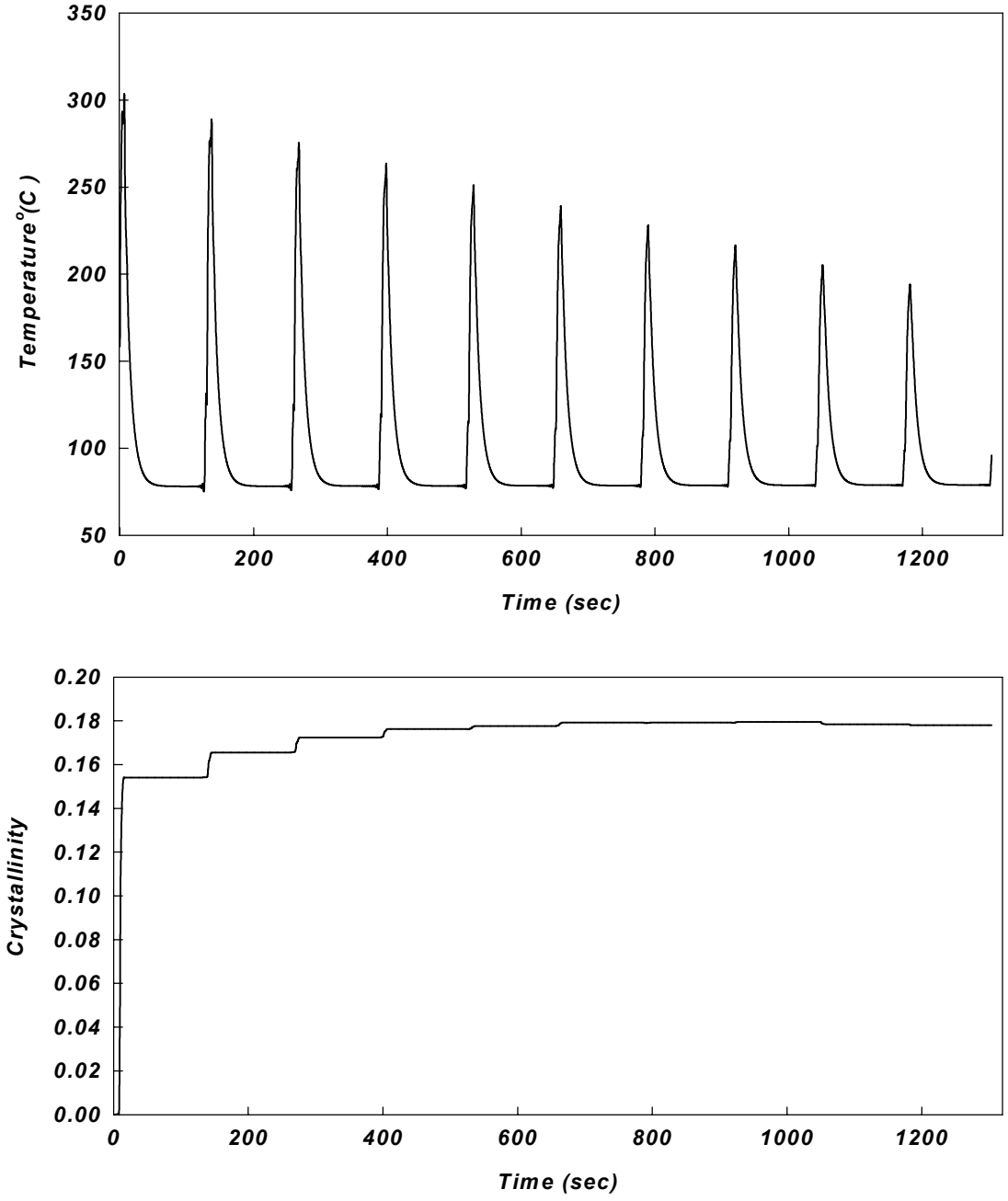

Figure 6.5 Temperature profiles for the top surfaces of the 20th ply during winding and the corresponding crystallinity development for the preheat temperature of 80 ^{o} C

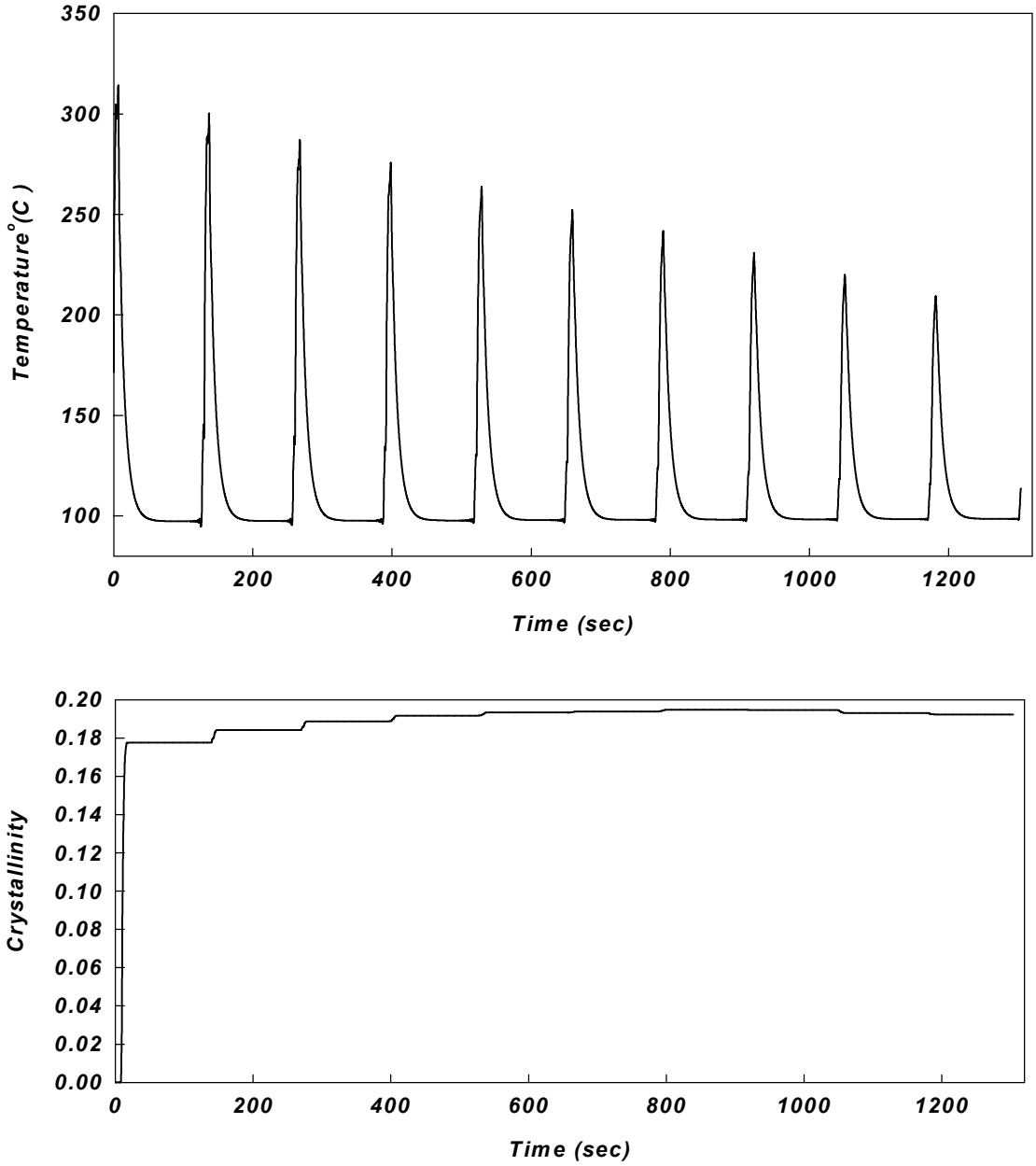

Figure 6.6 Temperature profiles for the top surface of the 20th ply during winding and the corresponding crystallinity developement for the preheat temperature of 100°C

Chapter 7 Conclusions and Future Work

7.1 Conclusions

In this investigation, a comprehensive model was developed to simulate the hot-gas heating on-line consolidation filament winding process. The model included heat transfer analyses of the composite substrate and the towpreg, consolidation of the composite substrate and the crystallization development of the composite matrix resin.

Two-dimensional finite element heat transfer analyses of the composite substrate and the towpreg were constructed to predict the temperature distribution in the composite and the temperature history during the on-line consolidation process. Both models were formulated with an Eulerian approach and solved in a quasi-steady state fashion. The models were used to study winding of graphite fiber, PEEK resin towpreg into composite cylinders. For the processing conditions studied, the hot-air heater does not create a molten zone on the surface of substrate cylinder but melts the resin on the surface of the towpreg at the nippoint. The mandrel winding speed was found to significantly affect the temperature distribution in the towpreg and the substrate. Lower winding speed yields higher temperature both in the substrate cylinder and in the towpreg.

An on-line consolidation model was constructed which included intimate contact and the autohesion of the interply interface formed as the incoming towpreg is laid on the surface of the composite substrate. The influence of the additional layers over the previously consolidated composite substrate was studied by combining the consolidation model with the heat transfer analysis. The model was verified with the experiment by Shih and Loos [22]. Model predictions of the temperature history and the degree of bonding compared well with the experimental data. The winding speed and the hot-gas temperature are two significant parameters that control consolidation. Slower winding speed or higher hot-gas temperature results in higher bonding strength hence better consolidation quality.

A model was used to study the crystallization behavior of PEEK resin involved in the complex phenomena of melting, cooling, remelting, resolidification and annealing in the filament winding process. Both the consolidation model and the crystallization

kinetics model are strongly dependent upon the temperature history experienced by the composite. Therefore, the heat transfer analysis, the consolidation model and the crystallization kinetics model were combined to study the on-line consolidation filament winding process and identify the relationships between the process variables and the structure quality. Lower winding speed or higher nozzle temperature yields higher nippoint temperature, better consolidation and higher crystallinity, which improve the quality of the composite structure. Preheating the substrate was also found to improve composite consolidation.

7.2 Future Work

The heat transfer analysis and experimental observation [22] show that the hot gas heater forms a melt zone on the surface of the towpreg. The surface of the substrate cylinder is heated to a temperature well below the melting temperature of PEEK resin. Hence, when the towpreg and the substrate cylinder enter the nippoint, heat transfer will occur due to the temperature difference. Further investigation should be devoted to this phenomenon.

Other important areas of work will be studying off-axis winding and manufacturing of large surface structure. The three-dimensional heat transfer model needs to be developed to study the heat conduction in axial direction.

References

[1] Ghasemi Nejhad, M. N. 1993. "Issues Related to Processability during the Manufacture of Thermoplastic Composites Using On-line Consolidation Techniques," *Journal of Thermoplastic Composite Materials*, 6:130-146.

[2] Zoller, P. 1988. "Solidification Processes in Thermoplastics and Their Role in the Development of Internal Stresses in Composites," *ASC 3rd Technical conference*, 439-448.

[3] Tzeng, J. T. and R. B. Pipes. 1992. "Thermal Residual Stress Analysis for In Situ and Post-Consolidated Composite Ring," *Composite Manufacturing*, 3(4): 273-279.

[4] White, S. R. And H. T. Hahn. 1992. "Process Modeling of Composite Materials: Residual Stress Development During Cure. Part I. Model Formulation," *Journal of Composite Materials*, 26 (16): 2402-2422.

[5] Coffenberry, B. S., D. E. Hauber and M. Cirino. 1993. "Low Cost Alternative: In-Situ Consolidated Thermoplastic Composite Structures," *38th International SAMPE Symposium*, 1640-1650.

[6] Ghasemi Nejhad, M. N., R. D. Cope and S. I. *Güceri* . 1991. "Thermal Analysis of In-situ Thermoplastic Composite Tape Laying," *Journal of Thermoplastic Composite Materials*, 4:20-45.

[7] Wells, G. M. And K. F. McAnulty. 1987. "Computer Aided Winding Using Non-Geodesic Trajectories," Proceedings, Sixth International Conference on Composite Materials, Second European Conference on Composite Materials, ICCM & ECCM, 1:1.161-1.173.

[8] Fazil O. Sonmez and H. Thomas Hahn. 1997. "Modeling of Heat Transfer and Crystallization in Thermoplastic Composite Tape Placement Process," *Journal of Thermoplastic Composite Materials*, 10:198-240.

[9] Beyeler, E. P. and S. I. *Güceri* . 1998. "Thermal Analysis of Laser Assisted Thermoplastic-Matrix Composite Tape Consolidation," *Journal of Heat Transfer*, 110: 424-430.

[10] Astrom, B. T. and R. B. Pipes. 1993. "A modeling Approach to Thermoplastic Pultrusion. Formulation of Models," *Polymer Composites*, 14(3):173-183.

[11] Grove, S. M. 1988. "Thermal Modeling of Tape Laying with continuous Carbon-Fiber-Reinforced Thermoplastics," *Composites*, 19:367-375.

[12] Mantell, S. C. and G. S. Springer. 1992. "Manufacturing Process Models for Thermoplastic Composites," *Journal of Composite Materials*, 26(16):2348-2377.

[13] Nejhad, M. N. G. 1993. "Issues Related to Processability during the Manufacture of Thermoplastic Composites Using On-Line Consolidation Techniques," *Journal of Thermoplastic Composite Materials*, 6:130-145.

[14] Pitchumani, R., R. C. Don, J. W. Gillespie and S. Ranganathan. 1994. "Analysis of On-line Consolidation during Thermoplastic Tow-Placement Process," in *Thermal Processing of Materials: Thermo-Mechanics, Controls and Composites* (ASME), HTD, 289:223-234.

[15] Sarrazin, H. and G. S. Springer. 1994. "Thermochemical and Mechanical Aspects of Composite Tape Laying," *Journal of Composite Materials*, 29(14):1908-1943.

[16] Nejhad, M. N. G., R. D. Cope and S. I. *Güceri* . 1991. "Thermal Analysis of In-Situ Thermoplastic Composite Tape Laying," *Journal of Thermoplastic Composite Materials*, 4:20-45.

[17] Nejhad, M. N. G., R. D. Cope and S. I. *Güceri* . 1991. "Thermal Analysis of In-Situ Thermoplastic Composite Filament Winding," *Transactions of the ASME*. 113:304-313.

[18] Nejhad, M. N. G., Gillespie, J. W. and Cope, R. D. 1992. "Processing Stresses for Thermoplastic Filament Winding using the Divergence Method," *Heat Transfer Effects in Materials Processing ASME*, 233:33-43.

[19] James, D. L. and Black, W. Z. 1996. "Thermal Analysis of Continuous Filament-Wound Composites," *Journal of Thermoplastic Composite Materials*, 9:54-75.

[20] James, D. L. and Black, W. Z. 1994. "Experimental Analysis and Process Window Development for Continuous Filament Wound APC-2," *Thermal Processing of Materials: Thermo-Mechanics, Controls and Composites ASME* 289:203-212.

[21] Dara, P. H. and Loos A. C. 1985. "Thermoplastic Matrix Composite Processing Model," *CCMS Report 85-10, Center for Composite Materials and Structures, Virginia Polytechnic Institute*

[22] Shih, P. J. and Loos, A. C. 1997. "On-Line Consolidation of Thermoplastic Composites," CCMS Report 97-06, *center for Composite Materials and Structures, Virginia Polytechnic Institute.*

[23] Lee, W. I. and Springer, G. S. 1987. "A model of the Manufacturing Process of Thermoplastic Matrix Composites," *Journal of Composite Materials*, 21:1017-1055.

[24] Mantell, S. C., Wang, Q. and Springer, G. S. 1992. "Processing Thermoplastic Composites in a Press and by Tape Laying – Experimental Results," *Journal of Composite Materials*, 26 (16): 2378-2401.

[25] Li, M. C. and Loos, A. C. 1994. "Thermoplastic Matrix Composite Processing Model," Center for Composite Materials and Structures, *Report CCMS-94-02, VPI-E-94-21,* Virginia Polytechnic Institute and State University, Blacksburg, Virginia.

[26] Fazil O. Sonmez and H. Thomas Hahn. 1997. "Analysis of the On-line Consolidation Process in Thermoplastic Composite Tape Placement," *Journal of Thermoplastic Composite Materials,* 10:543-572.

[27] Wool, R. P., B. L. Yuan and O. J. Mcgarel. 1989. "Welding of Polymer Interfaces," *Polymer Engineering and Science*, 29 (19): 1340-1367.

[28] Wool, R. P. and K. M. O'Connor. 1981. "A Theory of Crack Healing in Polymers," Journal of Applied Physics, 52 (10): 5953-5963.

[29] Kim, Y. H. and R. P. Wool. 1983. "A Theory of Healing at a Polymer-Polymer Interface Macromolecules," *Polymer Engineering and Science*, 16:1115-1120.

[30] Bastien, L. J. and J. W. Gillespie. JR. 1991. "A Nonisothermal Healing Model for Strength and Toughness of Fusion Bonded Joints of Amorphous Thermoplastics," *Polymer Engineering and Science*, 31(24): 1720-1730.

[31] Prager, S. and Tirrell M. 1981. "The Healing Process at Polymer-Polymer Interface," *The Journal of Chemical Physics*, 75:5194-5198.

[32] Wool, R. P. 1984. "Molecular Aspects of Tack," *Rubber Chemistry and Technology*, 57:307-309.

[33] Li, M. C. and A. C. Loos. 1992. "The Effects of Processing on Interply Bond Strength of Thermoplastic Composites," *Journal of Reinforced Plastics and Composites*, 11: 1142-1162.

[34] Davies, P., W. J. Cantwell, P. Y. Jar, H. Richard, D. J. Neville and H. Kausch. 1991. "Cooling Rate Effects in Carbon Fiber/PEEK Composites," *Composite Materials: Fatigue and Fracture*, Third Volume, ASTM STP 110:70-88.

[35] Folkes, J. J., G. Kalay and A. Ankara. 1993. "The Effect of Heat Treatment on the Properties of PEEK and APC-2," *Composites Science and Technology*, 46:77-83.

[36] Xiao, X. R., J. Denault and T. Vu-Khanh. 1992. "The Effect of Low Melt Temperature on Morphology and Mode-I Fracture Toughness of PEEK/Carbon Composite," *Journal of Thermoplastic Composite Materials*, 5:64-75.

[37] Cantwell, W., J. P. Davies and H. H. Kausch. 1990. "The Effect of Cooling Rate on Deformation and Fracture of IM6/PEEK Composites," *Composite Structures*, 14:151-171.

[38] Tregub, A., H. Harel and G. Marom. 1993. "The Influence of the Thermal History on the Mechanical Properties of Poly(Ether Ether Ketone) Matrix Composite Materials," *Composite Science and Technology*, 48:185-190.

[39] Talbott, M. F., G. S. Springer and L. A. Burglund. 1987. "The Effects of Crystallization on the Mechanical Properties of PEEK Polymer and Graphite Fiber Reinforced PEEK," *Journal of Composite Materials*, 21:1056-1081.

[40] Avrami, M. 1939. "Kinetics of Phase Change I, General Theory," *Journal of Chemical Physics*, 7:1103-1112.

[41] Avrami, M. 1940. "Kinetics of Phase Change II, Transformation-Time Relations for Random Distribution of Nuclei," *Journal of Chemical Physics*, 8:212-224.

[42] Avrami, M. 1941. "Kinetics of Phase Change III, Granulation, Phase Change and Microstructure," *Journal of Chemical Physics*, 9:177-184.

[43] Tobin, M. C. 1974. "Theory of Phase Transition Kinetics with Growth Site Impingement. I. Homogeneous Nucleation," *Journal of Polymer Science: Polymer Physics Edition*, 12:399-406.

[44] Tobin, M. C. 1976. "The Theory of Phase Transition Kinetics with Growth Site Impingement. II. Heterogeneous Nucleation," *Journal of Polymer Science: Polymer Physics Edition*, 14:2253-2257.

[45] Tobin, M. C. 1977. "The Theory of Phase Transition Kinetics with Growth Site Impingement. III. Mixed Heterogeneous-Homogeneous Nucleation and Noninternal Exponents of the Time," *Journal of Polymer Science: Polymer Physics Edition*, 15:2269-2270.

[46] Malkin, A. Y., V. P. Beghishev, I. A. Keapin and S. A. Bolgov. 1984. "General Treatment of Polymer Crystallization Kinetics-Part 1. A New Macrokinetic Equation and its Experimental Verification," *Polymer Engineering and Science*, 24(18): 1396-1401.

[47] Malkin, A. Y., V. P. Beghishev, I. A. Keapin and S. A. Bolgov. 1984. "General Treatment of Polymer Crystallization Kinetics-Part 2. A New Macrokinetic Equation and its Experimental Verification," *Polymer Engineering and Science*, 24(18): 1402-1408.

[48] Ozawa, T. 1971."Kinetics of Nonisothermal Crystallization," Polymer, 12:150-158.

[49] Maffezzoli, A. M., J. M. Kenny and L. Nicolais. 1989. "Welding of PEEK/Carbon Fiber Composite Laminates," *SAMPE Journal*, 25(1):35-39.

[50] Seferis, J. C. and C. N. Velisaris. 1986. "Modeling-Processing-Structure Relationships of Polyetheretherketone (PEEK) Based Composites," *Material Sciences for the Future. Society for the Advancement of Material and Process Engineering*, 1236-1253.

[51] Velisaris, C. N. and J. C. Seferis. 1988. "Heat Transfer Effects on the Processing-Structure Relationships of Polyetheretherketone (PEEK) Based Composites," *Polymer Engineering and Science*, 28:583-591.

[52] Nejhad, M. N. G., J. W. Gillespie and R. D. Cope Jr. 1992. "Prediction of Process-Induced Stresses for In-Situ Thermoplastic Filament Winding of Cylinders," Proceedings of 3rd International Conference, *Computer Aided Design in Composite Material Technology*, Newark, Delaware, Vol. 3, pp. 277-295.

[53] Choe, C. R. and K. H. Lee. 1989. "Nonisothermal Crystallization Kinetics of Poly(Etheretherketone) (PEEK)," *Polymer Engineering and Science*, 29(12):801-805.

[54] Bayley, F. J., Owen, J. M. and Turner, A. B. 1972. *Heat Transfer*. New York, Barnes & Noble.

[55] Hughes, J. R. Thomas. 1987. *The Finite Element Method: Linear Static and Dynamic Finite Element Analysis*. Prentice-Hall International, Inc.

[56] Blundell, D. J. ,Chalmers, J. M. , Mackenzie M. W. and Gaskin W. F. 1985. "Crystalline Morphology of the Matrix of Peek – Carbon Fiber Aromatic Polymer Composites I. Assessment of Crystallinity," *SAMPE Quarterly*, 16(4): 22-30.

Vita

Xiaolan Song was born on February 22, 1976. She attended Tsinghua University at Beijing, P. R. China from September of 1992 until July of 1997, receiving her Bachelor of Science Degree in Engineering Mechanics. Upon graduation, she entered the department of Engineering Science and Mechanics at Virginia Polytechnic Institute and State University and received the Master of Science degree in September of 2000. She is currently continuing for the Ph.D. degree in Engineering Science and Mechanics at Virginia Polytechnic Institute and State University.